The relaxational properties of compositionally disordered ABO_3 perovskites

2003 J. Phys.: Condens. Matter 15 R367

(http://iopscience.iop.org/0953-8984/15/9/202)

INSTITUTE OF PHYSICS PUBLISHING JOURNAL OF PHYSICS: CONDENSED MATTER

J. Phys.: Condens. Matter **15** (2003) R367–R411 PII: S0953-8984(03)35476-1

TOPICAL REVIEW

The relaxational properties of compositionally disordered ABO_3 perovskites

George A Samara

Sandia National Laboratories, Albuquerque, NM 87185, USA

Received 6 January 2003
Published 24 February 2003
Online at stacks.iop.org/JPhysCM/15/R367

Abstract

Random lattice disorder produced by chemical substitution in ABO_3 perovskites can lead to the formation of dipolar impurities and defects that have a profound influence on the static and dynamic properties of these materials that are the prototypical soft ferroelectric (FE) mode systems. In these highly polarizable host lattices, dipolar entities form polar nanodomains whose size is determined by the dipolar correlation length, r_c, of the host and that exhibit dielectric relaxation in an applied ac field. In the very dilute limit (<0.1 at.%) each domain behaves as a non-interacting dipolar entity with a single relaxation time. At higher concentrations of disorder, however, the domains can interact leading to more complex relaxational behaviour. Among the manifestations of such behaviour is the formation of a glass-like relaxor (R) state, or even an ordered FE state for a sufficiently high concentration of overlapping domains.

After a brief discussion of the physics of random-site electric dipoles in dielectrics, this review begins with the simplest cases, namely the relaxational properties of substitutional impurities (e.g., Mn, Fe and Ca) in the quantum paraelectrics $KTaO_3$ and $SrTiO_3$. This is followed by discussions of the relaxational properties of Li- and Nb-doped $KTaO_3$ and of the strong relaxors in the $PbMg_{1/3}Nb_{2/3}O_3$ and La-substituted $PbZr_{1-x}Ti_xO_3$ families. Some emphasis will be on the roles of pressure and applied dc biasing electric fields in understanding the physics of these materials including the R-to-FE crossover.

(Some figures in this article are in colour only in the electronic version)

Contents

1. Introduction

The ABO_3 perovskite oxides constitute an important family of ferroelectrics (FEs) whose relatively simple chemical and crystallographic structures have contributed significantly to our understanding of FE and antiferroelectric phenomena. They are the prototypical soft phonon mode systems that, in either pure or mixed crystal form, readily undergo structural phase transitions involving both polar and non-polar distortions of the cubic lattice shown in figure 1 [1, 2].

Random lattice disorder produced by chemical substitution in ABO_3 perovskites can lead to the formation of dipolar impurities and defects that have profound influence on the static and dynamic properties of these materials. Because of the high polarizability of the ABO_3 host lattice associated with the soft FE mode, dipolar entities polarize regions around them forming polar nano/microdomains whose size is determined by the temperature-dependent correlation length, r_c, of the host. When these dipolar entities possess more than one equivalent orientation, they may undergo dielectric relaxation in an applied ac field. In the very dilute limit (<0.1 at.%), each polar domain behaves as a non-interacting dipolar entity with a single relaxation time. At higher concentrations of disorder, the polar domains can interact leading to more complex relaxational behaviour with distributions of relaxation times. One manifestation of such behaviour is the formation of a glass-like relaxor state, or even an ordered FE state for a sufficiently high concentration of overlapping domains [3].

In this review we focus on the low-frequency ($\leqslant 10^7$ Hz) dipolar relaxational properties of disordered ABO_3 oxides that possess soft FE modes. Thus, we shall deal with the relaxations associated with the motion of dipolar entities and not with the much higher frequency lattice relaxation of these materials. We begin with the simplest cases, namely dipolar relaxations in the disordered quantum paraelectrics $KTaO_3$ and $SrTiO_3$ where the disorder is produced by dilute impurities or defects, and proceed to more complex perovskites. Much of this disorder is produced by chemical substitutions of ions of different valences than the host ions leading to the formation of lattice defects (figure 1). Among the simple substituents to be considered are Fe, Mn, Ca, Li and Nb.

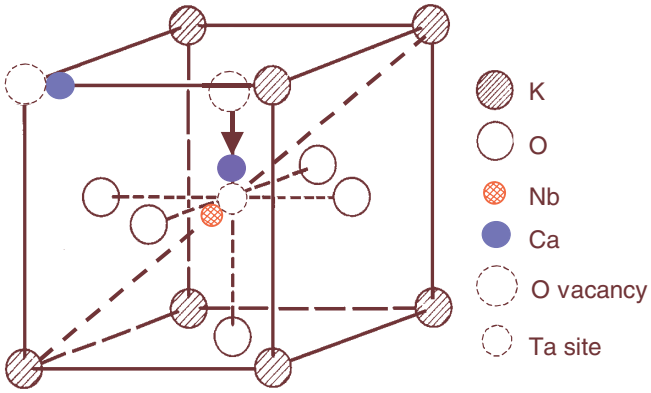

Figure 1. The cubic perovskite lattice showing the location of some substituents and vacancies.

2. Random-site electric dipoles in dielectrics

2.1. General considerations

The properties of random-site electric dipoles in dielectric host lattices as well as the possible collective behaviour of such dipoles have been topics of long-standing interest. Among the particularly important issues with respect to collective behaviour are the nature of the dipole–dipole interactions as a function of the polarizability of the host lattice and the possible formation of an ordered state at low temperatures.

For the ABO_3 oxides of present interest, the symmetry of the perovskite lattice (figure 1) makes it possible for the disorder-induced dipolar entities to generally have several equivalent orientations. Hopping among these orientations is manifested by dielectric relaxation under the influence of an applied ac electric field. In the simplest case of dilute systems where there is no interaction among dipoles, the relaxation is expected to be Debye-like with a single dipolar relaxation time, τ.

In the presence of dielectric losses and relaxations, the total dielectric response of the system in an ac field is described by the complex dielectric function

$$\epsilon = \epsilon' - \mathrm{i}\epsilon'', \tag{1}$$

where, in the Debye approximation, the real part ϵ' is given by the familiar expression [4]

$$\epsilon'(\omega) = \epsilon'_\infty + \frac{\epsilon'_s - \epsilon'_\infty}{1 + \omega^2\tau^2}, \tag{2}$$

and the imaginary part is given by

$$\epsilon''(\omega) = (\epsilon'_s - \epsilon'_\infty)\frac{\omega\tau}{1 + \omega^2\tau^2}. \tag{3}$$

In these equations ω is the angular frequency of the applied ac field, ϵ'_∞ is the high frequency dielectric constant (i.e., the dielectric constant in the absence of *dipolar* contributions, or the unrelaxed dielectric constant), and ϵ_s is the static, or relaxed dielectric constant. ϵ' and ϵ'' are related, at any given frequency, by the Kramers–Kronig dispersion relations [4]. The dielectric loss is proportional to ϵ'' and exhibits a maximum for $\omega\tau = 1$, i.e., for $\omega = 1/\tau$. It is customary to express the loss in terms of the loss tangent, $\tan\delta$ (where δ is the phase angle by which the polarization lags the applied field), which is given by

$$\tan\delta = \epsilon''(\omega)/\epsilon'(\omega) = \frac{(\epsilon'_s - \epsilon'_\infty)\omega\tau}{\epsilon'_s + \epsilon'_\infty\omega^2\tau^2}. \tag{4a}$$

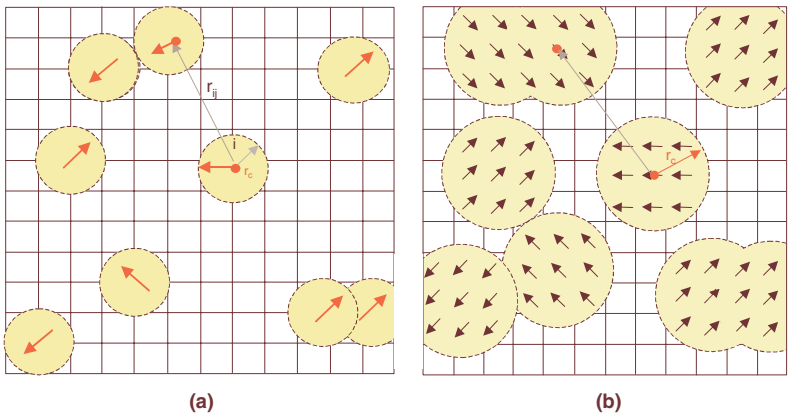

Figure 2. Contrasting the domain structure of a dipolar entity in a normal dielectric host lattice (a) and in a soft FE mode lattice (b). In (a) the dipole polarizes only the region in its immediate vicinity (correlation length $r_c \approx 1$ lattice constant) and behaves as an isolated dipole, whereas in (b) the dipole induces polarization in several unit cells around it (large r_c) forming a dipolar nanodomain.

For dielectrics with dilute dipolar impurities, $\epsilon'_s \approx \epsilon'_\infty$ and equation (4*a*) reduces to the form

$$\tan\delta = \left(\frac{\Delta\epsilon'}{\epsilon'_s}\right)\frac{\omega\tau}{1+\omega^2\tau^2}, \tag{4b}$$

where $\Delta\epsilon'$ is the difference between the relaxed and unrelaxed ϵ, i.e., the relaxation magnitude.

Since hopping between equivalent dipolar orientations is a thermally activated process, τ can be expected to obey the Arrhenius law

$$\tau^{-1} = \tau_0^{-1}\exp(-E/kT), \tag{5}$$

where τ_0 is the reciprocal of the attempt frequency, ω_0, and E is the activation energy. In terms of these considerations, the signature of dipolar relaxation is a peak in $\tan\delta$ versus T.

2.2. *Dipolar interactions—ordinary dielectric hosts*

For a system of random dipoles in an ordinary, i.e., weakly polarizable, dielectric medium, electrostatic considerations show that the anisotropic dipolar interaction is described by the Hamiltonian [5, 6]

$$H_{dd} = \frac{1}{\epsilon_0}\sum_{ij}\frac{1}{\boldsymbol{r}_{ij}^3}[\boldsymbol{d}_i^*\boldsymbol{d}_j^* - 3(\boldsymbol{n}_{ij}\boldsymbol{d}_i^*)(\boldsymbol{n}_{ij}\boldsymbol{d}_i^*)], \tag{6}$$

where

$$\boldsymbol{d}_i^* = \boldsymbol{d}_i[1+\gamma(\epsilon'_0-1)/3] \tag{7}$$

is the effective impurity dipole moment of dipole i (γ is the local field correction factor), $\boldsymbol{d}_i$ is the permanent dipole moment of the impurity, ϵ'_0 is the static dielectric constant of the pure crystal, r_{ij} is the separation distance between dipoles i and j and $\boldsymbol{n} = \boldsymbol{r}/r$, (figure 2(a)). Minimizing H with respect to possible directions of every dipole yields local energy minima defined by [7]

$$\boldsymbol{E}_i = \lambda_i\boldsymbol{d}_i, \tag{8}$$

where $\boldsymbol{E}_i$ is the effective local field (in energy units) acting on the ith dipole, and $\lambda_i \geqslant 0$ is the Lagrange factor corresponding to the conditional minimum of equation (6) at $|\boldsymbol{d}_i| =$ constant, [7]. Thus, in the metastable states at $T = 0$ K, the system consists of 'frozen' configurations of dipole moments each oriented along its local field. At finite T (but lower than the characteristic heights of barriers between metastable states), the local field determines the average thermal value of the dipole moment [7]. The random distribution of dipoles and the variable sign of the dipole–dipole interaction energy cause the local fields at the impurities to have different orientations, and at low temperatures the dipoles freeze into a state with zero net polarization in the absence of an applied field. This low temperature state is the *dipolar glass* state, which is in many ways analogous to the spin glass state.

An important question pertaining to impurity dipoles in ordinary dielectrics is whether or not such a system can exhibit long-range FE order at low temperatures. This question has been studied extensively [5–9], and it is now definitively established that FE order is not possible because the configurational average $\langle H_{dd} \rangle$ of equation (6) vanishes. Rather, the dipolar interaction favours a condensation at low temperature into an array of randomly oriented dipoles similar to a spin glass phase, as already noted above. This is a consequence of the fact that when the polarizability of the host is small, the fluctuations in the local field, $\boldsymbol{E}_{loc}$, become greater than the average local field, $\langle \boldsymbol{E}_{loc} \rangle$. In ordinary dielectrics, the correlation length for dipolar interactions, r_c, is small (of the order of a lattice constant), so that in the dilute limit $r_{ij} \gg r_c$. As the concentration n of dipoles increases, weak correlations among dipoles set in leading to the appearance of a maximum in the temperature dependence of the dielectric constant. This $\epsilon'(T)$ peak becomes sharper the higher the concentration of dipoles. The peak temperature, T_m, is given by [7]

$$kT_m \approx nd^{*2}/\epsilon_0'. \tag{9}$$

Dipolar glass behaviour of the type discussed above, occurs in alkali halides with dipolar impurities, e.g., CN^- and OH^- in KCl and KBr and Li^+ in KCl, where, in the latter case, the dipole is associated with the Li being off-site due to the large size mismatch between Li^+ and K^+. These materials have been studied extensively [8, 9]. At sufficiently high concentrations of dipoles, they exhibit $\epsilon'(T)$ maxima and weak polarization versus electric field hysteresis loops indicative of a degree of dipolar correlations [3, 8, 9].

2.3. Dipolar interactions—highly polarizable hosts

The case of dipolar defects in highly polarizable dielectric host crystals is more interesting. The best examples of such crystals are soft mode FEs of the perovskite type near their FE instabilities or phase transitions. This case has attracted much interest, and the qualitative picture that has emerged is as follows [3, 7]. The presence of a dipolar entity on a given lattice site in such hosts induces dipoles in a region determined by the correlation length, r_c, at that site. Within this correlation length, dipolar motion is correlated leading to the formation of a polar nanodomain (figure 2(b)). Thus, unlike for normal dielectrics, in this case dipolar entities are not point dipoles. The correlation length is determined by the polarizability of the host which is inversely proportional to the soft mode frequency, ω_s, [3], so that as $\omega_s \to 0$ on decreasing temperature, r_c diverges (inset figure 3). Figure 3 shows the temperature dependence of r_c for the model incipient FE $KTaO_3$ determined from the temperature dependence of ω_s, or of ϵ (since for soft mode systems $\omega_s^2\epsilon \approx$ constant [2]). As can be deduced from figure 3, at high temperature, r_c and the nanodomains are relatively small. With decreasing T, the rapidly increasing r_c greatly increases the size of the domains coupling them into growing polar domains (figure 2(b)) and increasing their Coulombic interactions. Ultimately, and if

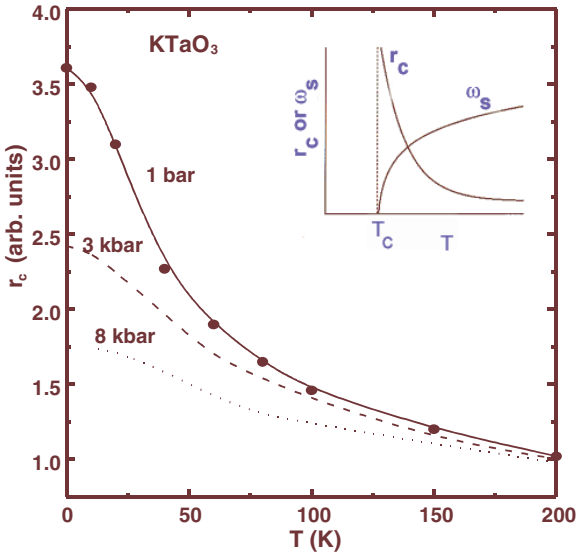

Figure 3. Temperature dependence of the correlation length for dipolar interactions (r_c) in a $KTaO_3$ host lattice showing the strong influence of pressure [3]. The inset shows schematically the vanishing of the FE soft mode frequency (ω_s) and the divergence of r_c on approaching the transition temperature (T_c).

the concentration, n, is sufficiently high, the domains will percolate (or permeate) the whole sample and precipitate a static, cooperative long-range ordered FE state at $T < T_c$. On the other hand, if n is not large enough, the domains will not induce a FE state; rather, a dynamic 'slowing down' of the dipolar fluctuations within each domain occurs at $T < T_m$ leading to a glass-like relaxor state. Such a state is characterized by a distribution of relaxation times related to the sizes of the nanodomains.

Vugmeister and Glinchuk (VG) considered this case of dipolar interactions in a highly polarizable host more formally [7]. They find that the high polarizability of the medium not only renormalizes the dipole moment of the impurity, but also functionally changes the dependence of the dipole–dipole interaction energy on the spacing between dipoles. Specifically, the anisotropic dipolar interaction given by equation (6) is modified by the addition of an isotropic component, which is determined by a strong indirect exchange-type interaction via the phonons of the host. This interaction is predominantly through the transverse optic (TO) phonons (particularly the soft FE mode), and its magnitude depends on the polarization correlation length, r_c. The Hamiltonian for the interaction between dipolar entities i and j in this case takes the form [7]

$$H^*_{dd} = -\tfrac{1}{2}\sum_{ij\alpha\beta} K^{\alpha\beta}_{ij}(r_{ij}) d^*_{i\alpha} d^*_{j\beta}, \tag{10}$$

where α, β are Cartesian coordinates and

$$K^{\alpha\beta}(r) = \frac{1}{\epsilon'_0}\left\{\left[\frac{2}{3}\frac{1}{rr_c^2}\exp(-r/r_c) + \frac{4\pi}{3V_0}\right]\delta_{\alpha\beta} + (3n_\alpha n_\beta - \delta_{\alpha\beta})\left[\frac{1}{r^3} - \exp(-r/r_c)\left[\frac{1}{r^3} + \frac{1}{r^2 r_c} + \frac{1}{rr_c^2}\right]\right]\right\} \tag{11}$$

where V_0 is the crystal volume, δ is the Kronecker delta and $\boldsymbol{n} = \boldsymbol{r}/r$ is the direction vector.

In this case of very large dielectric constants, $\epsilon_0' \gg 1$ so that the effective dipole moment of the dipolar entity, equation (7), becomes

$$\boldsymbol{d}^* = \gamma \epsilon_0' \boldsymbol{d}/3. \tag{12}$$

A key result is that the configurational average, $\langle H_{dd}^* \rangle$, for this polar phonon-mediated interaction does not vanish making it possible for polar nanoregions to interact cooperatively to achieve long-range FE order. The strength of this interaction, $J(r)$, varies exponentially with distance as

$$J(r) = J_0 \exp(-r/r_c). \tag{13}$$

The FE state is ushered by the appearance of a non-zero mean dipole moment, and, in mean field approximation, the transition temperature, T_c, is given by [7]

$$kT_c = \left(\frac{4\pi}{3}\right)\frac{d^{*2}n}{\epsilon_0'(T_c)} = \left(\frac{4\pi}{27}\right)\gamma^2 d^2 n \epsilon_0'(T_c), \tag{14}$$

where ϵ_0' is the value of ϵ' at T_c.

VG find that for dipolar entities in highly polarizable lattices there are two limiting cases, expressed in terms of the quantity nr_c^3, where n is the impurity concentration [7]:

Case 1

$nr_c^3 < N^*$, i.e., the low concentration limit where the separation r between dipoles is greater than r_c, and N^* is a characteristic quantity for a given material system. In this case, spatially inhomogeneous fluctuations of the polarization suppress FE order, and the dipolar nanoregions form a dipolar glass-like, or relaxor state at low temperature with some correlation among nanoregions. In the extreme case where $r \gg r_c$, i.e., in the very dilute limit, there is no correlation and the low T state is a dipolar glass akin to that in normal dielectric hosts.

Case 2

$nr_c^3 > N^*$, i.e., the high concentration limit where r_c is greater than the mean separation between dipoles. In this case, the crystal undergoes a FE phase transition accompanied by spontaneous polarization given by $\langle P \rangle = n\langle d^* \rangle$.

The crossover between the two cases is given by $nr_c^3 = N^*$ (or $n = N^*/r_c^3 = N^*/V_c$), where V_c is the correlation volume which can be expressed in units of the unit cell volume, V. For an ordinary polarizable crystal $r_c \approx a$, the lattice parameter, but for a highly polarizable soft optic mode lattice $r_c \gg a$, and it is strongly T dependent. Specifically, as noted earlier,

$$r_{c(T)} \propto [1/\omega_s(T)] \propto \sqrt{\epsilon'(T)}. \tag{15}$$

A schematic T versus nr_c^3 phase diagram for such a system of polar nanodomains in a highly polarizable medium is shown in figure 4. For $nr_c^3 < N^*$ the system exhibits a dipolar glass-like or relaxor phase which transforms on heating to a paraelectric (PE) phase. For $nr_c^3 > N^*$, however, the low temperature ground state is FE and transforms to the PE phase on heating.

2.4. Relaxor versus normal ferroelectric

Relaxor behaviour in FE materials, that has been observed and studied most extensively in disordered ABO_3 perovskites, has been one of the hot recent topics in ferroelectricity [3]. A universal signature of the relaxor state is a broad frequency-dependent peak in the real

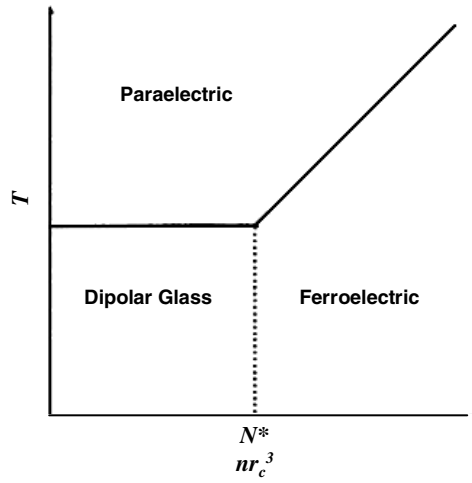

Figure 4. Schematic temperature–dipolar interaction phase diagram showing the relationships among the dipolar glass, FE and paraelectric phase.

part of the temperature-dependent dielectric susceptibility, χ' or $\epsilon'(\epsilon' = 4\pi\chi')$. The peak, which shifts to higher temperatures with increasing frequency, defines a dynamic freezing or glass-like transition temperature, T_m. The strong frequency dispersion in $\epsilon'(T)$ on the low-temperature side of T_m is associated with the slowing down of dipolar fluctuations within the polar nanodomains. At sufficiently low temperature all dipolar motion freezes, and the dispersion vanishes. We should also note that relaxor behaviour is also manifested by a frequency-dependent peak in the imaginary part of the dielectric constant ϵ'', or in $\tan\delta$. In this case the strong frequency dispersion is on the high-temperature side of the $\epsilon''(T)$ peak, a fact that can be inferred from the fact that ϵ' and ϵ'' are related by the Kramer–Kronig relations.

As already noted, relaxor behaviour is associated with the presence of polar nanodomains. Indeed, such nanodomains have been observed in many ABO_3 relaxors at temperatures far above the peak in $\epsilon'(T)$, and their occurrence is now considered to be crucial to the understanding of the properties of relaxors [3]. We picture a distribution of sizes of such nanodomains in which the orientational degrees of freedom are correlated within each domain, but uncorrelated across the various domains. Two important characteristics of this relaxor state, which distinguish it from simple dipolar glasses or spin glasses, are the existence of the dipolar nanodomains (versus individual dipoles or spins) and the presence of some degree of correlations among domains and cooperative freezing of the orientational degrees of freedom. Evidence for such cooperative effects comes from the observation of some remanent polarization in (polarization versus) electric field hysteresis loops as well as in deviation from Curie–Weiss behaviour in the temperature dependence of ϵ' and other properties [3].

In order to understand relaxors, it is useful to contrast some of their properties with those of normal FEs. We do so with the help of figure 5. The contrast is as follows:

- The P–E hysteresis loop (figure 5(a)) is the signature of a FE in the low temperature FE phase. The large remanent polarization, P_R is a manifestation of the cooperative nature of the FE phenomenon. A relaxor, on the other hand, exhibits a so-called slim loop, as shown on the right-hand side. For sufficiently high electric fields the nanodomains of the relaxor can be oriented with the field leading to large polarization; however, on removing

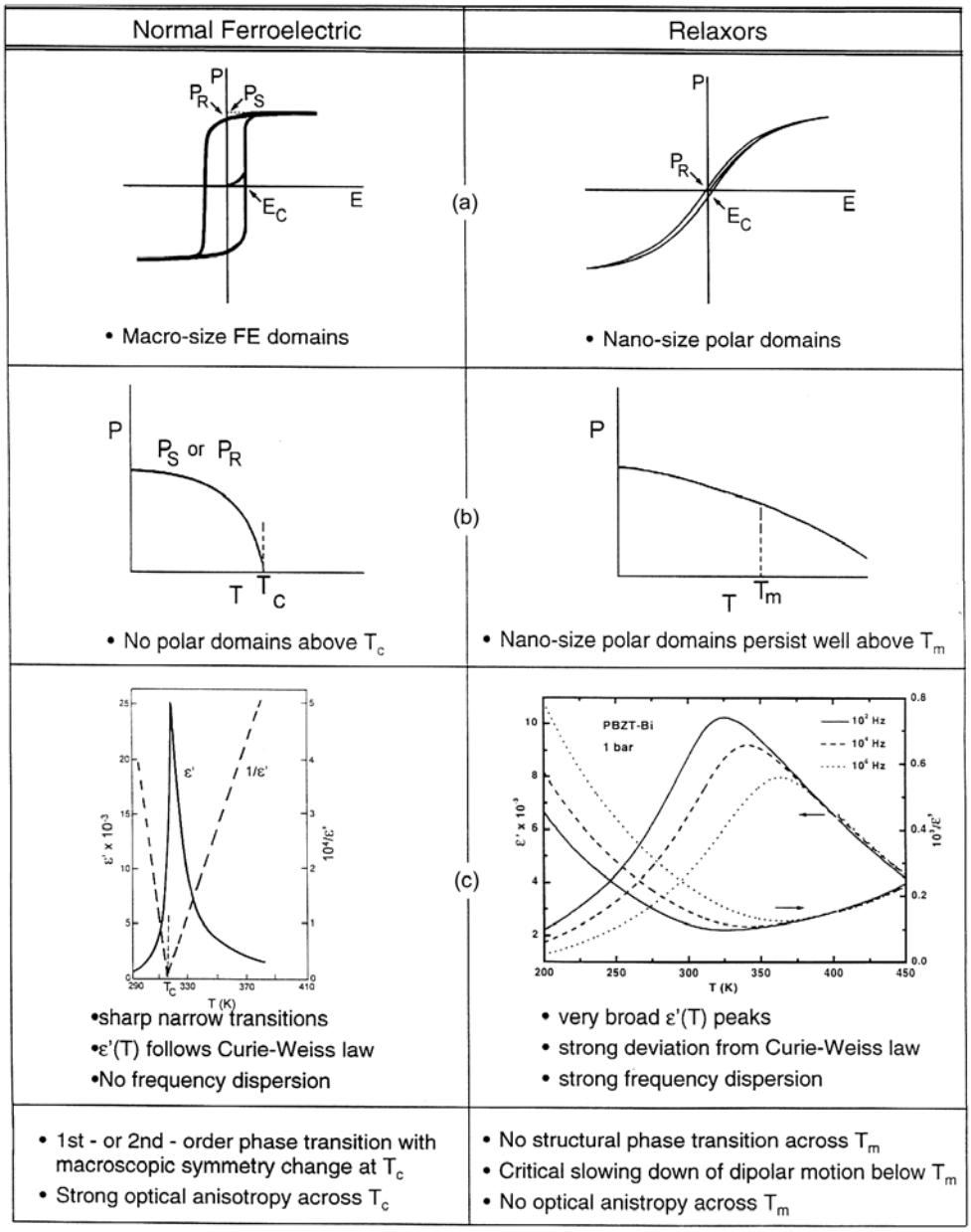

Figure 5. Contrast between the properties of normal FEs and relaxors.

the field most of these domains re-acquire their random orientations resulting in a small P_R. The small P_R is evidence for the presence of some degree of cooperative freezing of dipolar (or nanodomain) orientations.

- The saturation and remanent polarizations of a FE decrease with increasing temperature and vanish at the FE transition temperature (T_c). The vanishing of P at T_c is continuous for a second-order phase transition (figure 5(b)) and discontinuous for a first-order transition.

No polar domains exist above T_c. By contrast, the field-induced polarization of a relaxor decreases smoothly through the dynamic transition temperature T_m and retains finite values to rather high temperatures due to the fact that nano-size polar domains persist to well above T_m.

- The static dielectric susceptibility, or dielectric constant (ϵ') of a FE exhibits a sharp, narrow peak at T_c (figure 5(c)). For a single crystal the peak is very sharp and the width at half max is ∼10–20 K. For a mixed oxide FE, e.g., a PZT, the peak is somewhat rounded due to compositional fluctuations, and the width at half max is typically ∼20–40 K. The FE response is frequency independent in the audio frequency range. By contrast a relaxor exhibits a very broad $\epsilon'(T)$ peak and strong frequency dispersion in the peak temperature (T_m) and in the magnitude of ϵ' below T_m. The conventional wisdom has been that the broad $\epsilon'(T)$ peak, also referred to as a 'diffuse phase transition', is associated with compositional fluctuations leading to many micro FE regions with different compositions and T_cs. However, it has been clearly demonstrated through pressure experiments that this is not the case [3]. The breadth of the peak is simply a manifestation of the dipolar glass-like response of these materials.
- The temperature dependence of ϵ' of a FE obeys a Curie–Weiss law, $\epsilon' = C/(T - T_0)$, above T_c as shown by the linear $1/\epsilon'$ versus T response in figure 5(c). By contrast $\epsilon'(T)$ of a relaxor exhibits strong deviation from this law for temperatures of many tens to a few hundred degrees above T_m. It is only at very high temperatures that a linear $1/\epsilon'$ versus T response is obtained.
- The FE transition can be thermodynamically first or second order and involves a macroscopic symmetry change at T_c. Transparent FEs exhibit strong optical anisotropy across T_c. By contrast, there is no structural phase transition across T_m in a relaxor. The peak in $\epsilon'(T)$ is simply a manifestation of the slowing down of the dipolar motion below T_m. For transparent relaxors, there is no optical anisotropy across T_m.

The above discussion makes it very clear that the properties and physics of relaxors are very different from those of normal FEs. We shall discuss the properties and physics of a number of relaxors in later sections.

3. Dipolar relaxations in simple quantum paraelectrics

The incipient FEs, undoped $KTaO_3$ and $SrTiO_3$ are model quantum paraelectrics at low temperatures. At high temperatures, both have the ideal cubic perovskite structure (figure 1) and exhibit classic FE soft mode behaviour, a long wavelength transverse optic (TO) phonon mode whose frequency ω_s decreases (softens) with decreasing temperature. Although for both crystals ω_s tends to zero as $T \to 0$ K, it is prevented from vanishing by quantum fluctuations which stabilize the high temperature phase to the lowest temperatures (millikelvins). Thus, $KTaO_3$ remains cubic, and $SrTiO_3$, which exhibits an antiferrodistortive cubic-to-tetragonal transition at ∼105 K, retains its tetragonal structure at low temperatures [1, 2]. The influence of quantum fluctuations on the dielectric response of these materials is manifested by deviations from the Curie–Weiss response of $\epsilon'(T)$ at low temperatures, culminating in a high, temperature-independent ϵ' below ∼3 K (figure 6). The high value ϵ' and the flat $\epsilon'(T)$ response are signatures of a quantum paraelectric state [3].

Lattice disorder produced by chemical substitution at both the A and B sites in $KTaO_3$ and $SrTiO_3$ can lead to the formation of dipolar entities and associated dipolar relaxations. In the dilute limit (<0.1 at.1%), these entities behave as non-interacting dipolar nano/microregions, whereas at higher concentrations they can lead to the formation of either a dipolar-glass or a

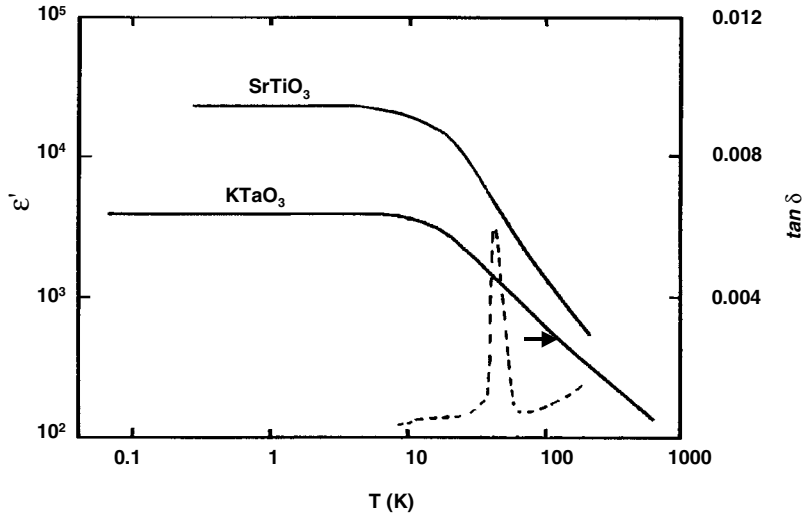

Figure 6. Temperature dependences of ϵ' at 1 bar of $SrTiO_3$ (adapted from [11]) and of $KTaO_3$ (adapted from [10]) showing the quantum paraelectric state where ϵ' is independent of temperature. Also shown for $KTaO_3$ is the 40 K dielectric loss ($\tan\delta$) peak [10].

FE state. In this section we shall examine the influence of several substituents on the dielectric and relaxational properties of $KTaO_3$ and $SrTiO_3$. We start with 'pure' $KTaO_3$.

3.1. 'Pure' $KTaO_3$

Nominally pure, cubic $KTaO_3$ is not expected to exhibit any of the dipolar relaxational effects of present interest. However, it has long been known that this material exhibits anomalous behaviour, e.g., in its thermal conductivity and Raman spectra [10]. Most notable is the observation of first-order lines in the Raman scattering spectrum (forbidden in a cubic lattice where each lattice site is a centre of inversion symmetry) that implicate symmetry-breaking local disorder. The atomic origin of this disorder has been the subject of much investigation and remains incompletely settled. From an early study of the temperature dependence of the Raman spectra, Uwe *et al* [12] concluded that the first-order Raman lines originate from FE microregions (FMRs) that exist in the crystal, a conclusion that has generally been accepted [10, 13, 14]. But what is the atomic origin of these FMRs?

Another anomalous property of 'pure' $KTaO_3$ is the observation of a dielectric loss, $\tan\delta(T)$, peak at ∼40 K at 1 kHz which has been studied by several authors [10, 15, 16]. Salce *et al* [10] results are shown in figure 6 and in more detail in figure 7 where it is seen that the amplitude of the peak is very strongly sample dependent, being smallest for the 'ultra pure' samples. Note from figure 6 that there is no visible anomaly in the real part of the dielectric function accompanying this peak. Undoubtedly, this dielectric loss peak is the signature of a dipolar impurity or defect, and this was confirmed by measurements of the frequency dependence of the peak [10, 15, 16]. Figure 8 is an Arrhenius plot showing the temperature dependence of the relaxation frequency for an 'ultra pure' sample according to Salce *et al* [10]. The Arrhenius nature of the response points to the non-interacting point-like, single relaxation time character of the responsible dipolar defect. Fit of these data to equation (5) yields the parameters $E = 440$ K $= 38$ meV and $1/\tau_0^{-1} \cong 1 \times 10^{11}$ Hz which are compared in table 1 with similar parameters obtained by others [15, 16] on 'pure' crystals. We note that Salce *et al*

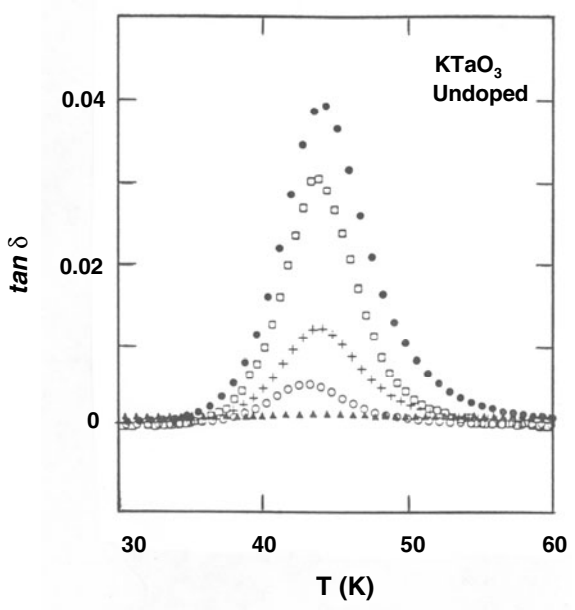

Figure 7. The dielectric losses around 40 K (at 1 kHz) for five nominally pure $KTaO_3$ crystals (after [10]).

[10] values of E and τ^{-1} are considerably smaller than those reported by the other authors. The cause of the numerical discrepancies is not known. Additionally, with the exception of Salce *et al* result, values of E in table 1 range from 70–90 meV suggesting that more than one dipolar centre may be involved in 'pure' $KTaO_3$ [16]. We should also note that Laguta *et al* [16] find that the dielectric feature at ∼40 K consists of two $\tan\delta$ peaks (at ∼40 and 48 K at 10 kHz) for both their 'pure' and Fe-doped samples (see table 1). Both peaks exhibit simple Arrhenius kinetics with distinctly different E's (table 1).

The $\tan\delta(T)$ anomaly near 40 K has also been observed with varying amplitudes in samples intentionally doped with Fe and Mn with essentially the same Arrhenius parameters [10, 15, 16][1]. Iron doping resulted in the most intense peaks, and Fe has often been implicated in the 40 K anomaly. It has also been suggested that this loss feature may be associated with some off-stoichiometry in the crystal, and the oxygen vacancy has been suggested as a likely candidate [10, 16]. Annealing in oxygen studies appear to confirm the involvement of the oxygen vacancy [10]. Salce *et al* [10] performed an evaluation of the then available thermal conductance, dielectric, EPR, optical and annealing results on both undoped and intentionally doped $KTaO_3$ crystals and concluded:

(i) the dielectric loss peak and the other cited anomalous properties of 'pure' $KTaO_3$ originate from the same source, namely the distorted FMRs, and
(ii) the responsible dipolar defect is an extended defect of rhombic symmetry involving an Fe^{3+} ion associated with an oxygen vacancy.

Laguta *et al* [16] have questioned the latter conclusion. By analysing ESR spectra over the range 4–500 K they concluded that the rhombic Fe centres are *static* dipole centres over this temperature range and thus cannot be responsible for the observed relaxation near 40 K. These

[1] The Fe-doped crystal has two additional tan $\delta(T)$ peaks associated with the iron, and the Mn-doped crystal has one additional peak associated with the manganese.

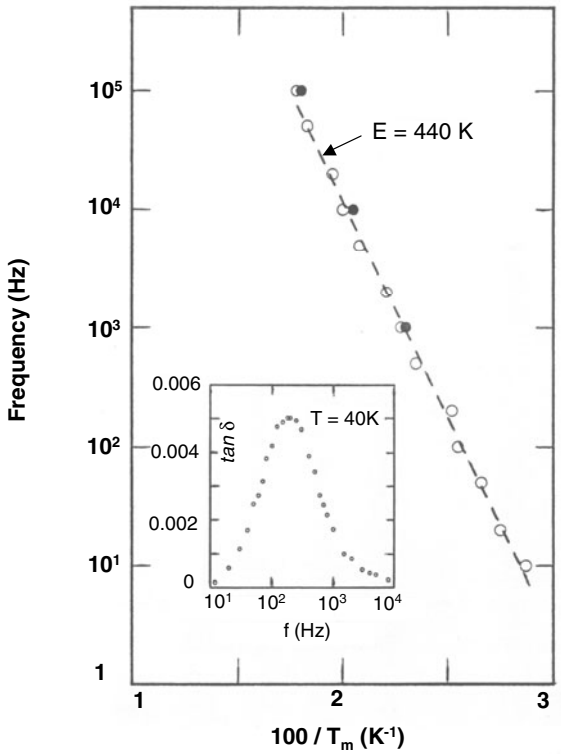

Figure 8. Arrehenius plot of the temperature dependence of relaxation frequency for an undoped (○) and an Fe-doped $KTaO_3$ crystal (●). The inset shows the loss peak at 40 K (after [10]).

authors went on to note that the reorientation parameters of Li^+ in KT obtained from NMR studies [19] are almost the same as those for the 48 K (at 10 kHz) loss peak (see table 1). They, thus, implicate Li^+ at $\leqslant$0.01 at.% which would be very difficult to detect by the usual analytical tools.

While the atomic nature of the dipolar centre(s) responsible for the ∼40 K relaxational feature (or features) remains unsettled, it is certain that it is associated with an unavoidable impurity or lattice defect. Indeed, given the very low concentrations of the responsible defect(s) the nature of the defect may never be known. One thing is clear, however; in the highly polarizable KT host lattice with its long correlation length, each dipolar defect is capable of polarizing a relatively large region around it at low temperatures and thereby forming a polar nanoregion. At the very low concentrations involved, these nanoregions are sufficiently far apart that there are no correlations among their dipolar fluctuations, and they exhibit simple Debye relaxations.

3.2. Transition metal dopants in $KaTO_3$: off-centre Mn, Fe, Ni and Co

The defect structure and relaxational properties of $KaTO_3$ doped with divalent and trivalent iron group transition metal ions have been investigated by dielectric spectroscopy and EPR. Dilute doping at the 0.01–0.1 at.% level produces dopant-induced frequency-dependent dielectric loss peaks.

Results for a 0.01 at.% Mn^{2+}-doped $KaTO_3$ crystal are shown in figure 9 [16]. It is seen that the real part of the susceptibility, ϵ', decreases smoothly with increasing T as for 'pure'

Table 1. Arrhenius parameters for various Debye relaxations in undoped and doped $KTaO_3$ crystals. Also listed are the ionic radii of the various dopants.

Sample	ri (Å)	Peak T (K)	E (meV)	τ_0^{-1} (s^{-1})	Reference
(a) Low-temperature (∼40 K) relaxation: undoped samples					
$KTaO_3$ 'ultra pure'		43 @ 1 kHz	38	$\sim 1 \times 10^{11}$	[10]
$KTaO_3$ undoped		43 @ 1 kHz	72	3×10^{12}	[15]
$KTaO_3$ undoped		39.5 @ 1 kHz	73.6	6.7×10^{13}	[17]
$KTaO_3$ undoped		39 @ 1 kHz	69	1.5×10^{13}	[16]
$KTaO_3$ undoped		48 @ 1 kHz	86	4.7×10^{13}	[16]
(b) Low-temperature (∼40 K) relaxation: doped samples					
$KTaO_3$–1.5 at.% Nb	0.69	39 @ 1 kHz	70.6	—	[17]
$KTaO_3$–1.5 at.% Fe	0.74		90	1.6×10^{13}	[18]
$KTaO_3$–1.5 at.% Li	0.68		87	3.3×10^{13}	[18]
$KTaO_3$–1.5 at.% Li	0.68	^{7}Li NMR	86	5×10^{13}	[19]
$KTaO_3$–1.5 at.% Fe	0.74	41 @ 10 kHz	72	2.3×10^{13}	[16]
$KTaO_3$–1.5 at.% Fe	0.74	48.5 @ 10 kHz	84	2.2×10^{13}	[16]
$KTaO_3$–1.5 at.% Fe	0.74	40.3 @ 10 kHz	70	2×10^{13}	[16]
$KTaO_3$–1.5 at.% Fe	0.74	48 @ 10 kHz	83	2.7×10^{13}	[16]
(c) Higher temperature relaxations: doped samples					
$KTaO_3$ Mn^{2+}	0.80	56 @ 1 kHz	110	5×10^{13}	[15]
$KTaO_3$ Mn^{2+}	0.80	55 @ 1 kHz	110	5×10^{13}	[16]
$KTaO_3$ Co^{2+}	0.73	186 @ 1 kHz	360	4×10^{13}	[15]
$KTaO_3$ Ni^{3+}		193 @ 1 kHz	400	1.5×10^{13}	[15]
$KTaO_3$ Fe^{3+}	0.64	184 @ 1 kHz	350	3×10^{13}	[15]
$KTaO_3$ Fe^{3+}	0.64	185 @ 1 kHz	340	3.3×10^{13}	[16]
$KTaO_3$ Fe^{2+}	0.74	149 @ 1 kHz	300	8×10^{13}	[15]
$KTaO_3$ Fe^{2+}	0.74	150 @ 1 kHz	300	1×10^{14}	[16]

KT, but the imaginary part, $\epsilon''(= \epsilon' \tan\delta)$, exhibits two peaks, at 43 and 56 K at 1 kHz. The former is the omnipresent peak observed in 'pure' $KTaO_3$ samples (as discussed above), and the latter is associated with the presence of the Mn^{2+} ion. The inset in figure 9 shows the frequency dispersion in both peaks for another Mn^{2+}-doped crystal [15], where the data are plotted as $\tan\delta$ versus $1/T$. Analysis of the frequency dependence of the 56 K peak reveals that it is a nearly ideal Debye peak involving a single relaxation time and implying that it is due to a relatively simple, isolated (i.e., non-interacting) defect. The symmetric shape of the peak in the figure 9 inset is characteristic of such a defect.

Similar loss peaks are observed for Co^{2+}-, Ni^{3+}- and Fe^{3+}-doped $KTaO_3$ crystals [15, 16]. In the case of Fe-doping the spectrum reveals two $\tan\delta(T)$ peaks at 150 and 185 K in addition to the omnipresent 43 K peak. Results for a 0.3 at.% Fe-doped crystal are shown in figure 10 [16]. Again there are no anomalies in $\epsilon'(T)$. Annealing such Fe-doped crystals in a reducing (CO_2 + CO) atmosphere essentially eliminates the 185 K peak and enhances the 150 K peak, suggesting that the former is associated with Fe^{3+} and the latter with Fe^{2+} [15, 16], a conclusion supported by ESR results [16]. For all the above ions, the relaxation manifested in the $\tan\delta(T)$ peak is found to be a simple Debye process with a single relaxation time. Table 1 summarizes the activation energy, (E), and pre-exponential factor, (T_0^{-1}), for this process deduced from a fit of the dielectric measurements to equation (5). That essentially a single relaxation process defines the dipolar hopping process for these materials can be seen

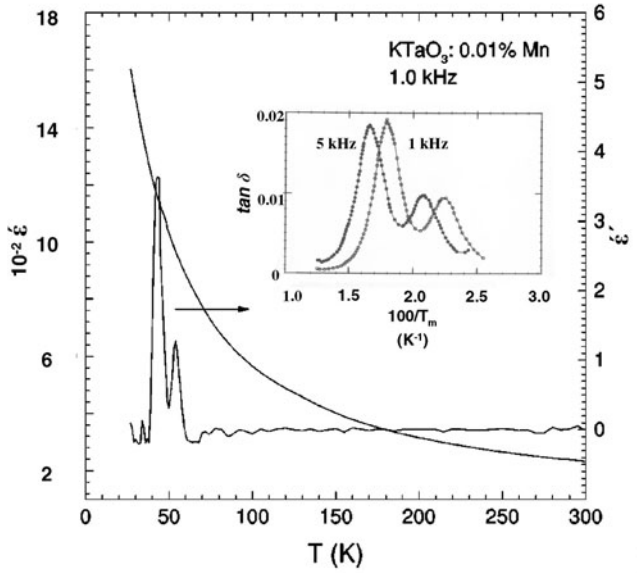

Figure 9. Temperature dependences of the real (ϵ') and imaginary (ϵ'') parts of the dielectric constant of a Mn-doped $KTaO_3$ crystal (0.01 at.% Mn) measured at 1 kHz (after [16]). The inset shows the frequency dispersion in the loss versus $1/T$ peaks for a Mn-doped $KTaO_3$ crystals (after [15]).

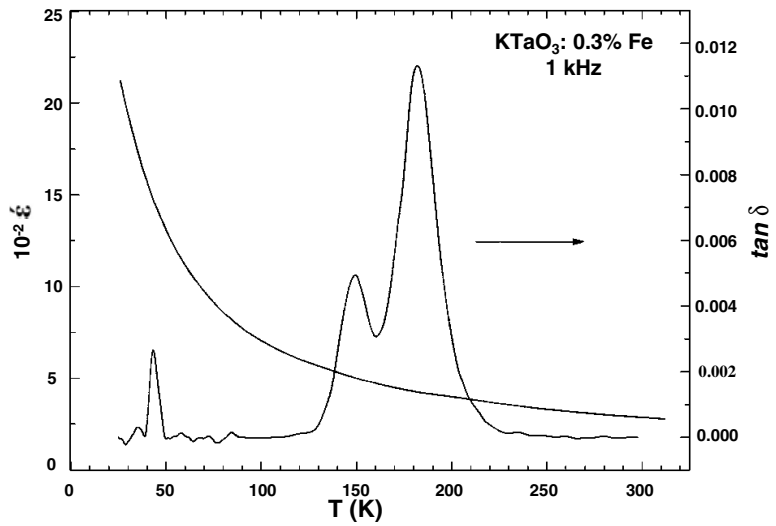

Figure 10. Temperature dependences of ϵ' and tan δ of an Fe-doped $KTaO_3$ crystal (0.3 at.% Fe) measured at 1 kHz (after [16]).

in the following way. From equations (4*b*) and (5) we note that a plot of $\tan\delta$ versus $1/T$ gives a symmetric peak for a Debye process. The width $\Delta(1/T)$ at half maximum of this peak is given by $\Delta(1/T) = 2.635\ \mathrm{K}/E$ [15]. Nowick *et al* [15] find that the activation energies deduced from this expression agree with Es deduced from Arrhenius plots, again emphasizing

the simple Debye-like character of the relaxation. A distribution of relaxation times would lead to wider $\tan\delta$ versus $(1/T)$ peaks and smaller Es.

So, what is the nature of the defects responsible for these relaxations? Let us first speculate about what might be expected from the doping. Intuitively, these transition metal ions might be expected to substitute for K^+ at the A site (figure 1). However, size considerations (ionic radii, $r_i \leqslant 0.80$ Å for all the ions in question (table 1) versus 1.33 Å for K^+) could make this substitution unfavourable. Alternatively, these divalent and trivalent ions could substitute for Ta^{5+} ($r_i = 0.68$ Å) at the B site. Indeed, early ESR studies of Mn^{2+}-, Cu^{2+}- and Co^{2+}-doped $KTaO_3$ crystals were interpreted to indicate substitution at the B site [20, 21].

To preserve charge neutrality on substitution for Ta^{5+}, the M^{2+} and M^{3+} ions would be accommodated by the formation of oxygen vacancies (V_0):1.5 V_0s for each M^{2+} and one V_0 for each M^{3+}. Reference to figure 1 shows that this substitution leads to the formation of a $\langle 100\rangle$M:V_0 pair defect on adjacent B and O sites. This pair is an electric dipole, which in the ABO_3 lattice has six equivalent positions and may thus undergo reorientation among these positions. Such reorientation can take place simply by the hopping of the vacancy among the oxygen sites. The dielectric loss peaks were attributed to such pair defects [15], a conclusion that was supported by the early ESR studies on the divalent dopants [20, 21] which reveal $\langle 100\rangle$ axial spectra confirming the existence of such a pair defect and its reorientation.

An additional feature relevant to the present work is the fact that the M^{2+} (or M^{3+}) and V_0 have opposite effective charges and can thus be expected to be drawn together by Coulombic attraction. Indeed, the early ESR work on the transition metal–V_0 pairs in perovskites, showed that the metal ion (e.g., M_n^{2+} in $SrTiO_3$) moves by a substantial distance (0.2 A) towards the oxygen vacancy [22]. The important point here is that the metal ion does not sit at a centre of symmetry, but is off-centre.

ESR should in principle lead to definitive identification of the symmetry and dipole orientation of paramagnetic transition metal ion dopants such as Mn^{2+} and Co^{2+}, since the crystal fields at the A and B sites in the ABO_3 lattice are distinct. Consequently, the fine structures in the ESR spectra of the paramagnetic ion will reflect the symmetry and environment of the particular occupied site. In reality, however, substitution can occur on more than one site and interpretation of the ESR spectra of the paramagnetic ions can be fairly involved. More recent and more detailed results on Mn^{2+}- and Fe^{3+}-doped KT [16] have led to different interpretations than the earlier results [20, 21].

Laguta *et al* [16] have measured ESR spectra at low temperatures on the same Mn^{2+}-doped KT samples used for their dielectric studies. Spectra of three magnetically non-equivalent centres of Mn^{2+} with axes along $\langle 001\rangle$ directions were observed, and the intensities of the spectral lines correlated with the intensity of the $\tan\delta$ peak at 55 K. Additional insight was obtained by investigating the influence of external electric fields, $\boldsymbol{E}$, on the ESR spectra. It is found that application of $\boldsymbol{E}$ parallel to the [001] axis leads to an enhancement of the intensity of the ESR lines of the Mn^{2+} centre with axis parallel to $\boldsymbol{E}$ and a decrease in the intensities of the other two centres. A particularly interesting set of results is shown in figure 11 for a sample with 0.01 at.% Mn measured at 26 K. The figure also shows the geometry of the sample as well as the orientation of the magnetic field, θ, for the measurement relative to the [001] axis; specifically $\theta = 78°$. Spectra at $\boldsymbol{E} = 0$ and 10 kV cm^{-1} are shown. Note the strong increase with increasing $\boldsymbol{E}$ in the intensity of the spectrum for which the centre axis is along $\boldsymbol{E}$ as represented by the $-5/2 \leftrightarrow -3/2$ transitions and the complete disappearance of the spectrum, represented by the $-3/2 \leftrightarrow -1/2$ transition at $\boldsymbol{E} = 10$ kV cm^{-1}, for the centres with axes perpendicular to $\boldsymbol{E}$. These results thus show that the dipoles associated with the Mn^{2+} defect can be reoriented by an external $\boldsymbol{E}$ field. At low temperatures (<27 K) the reoriented dipoles remain essentially frozen in place on removing $\boldsymbol{E}$, but at higher Ts, they

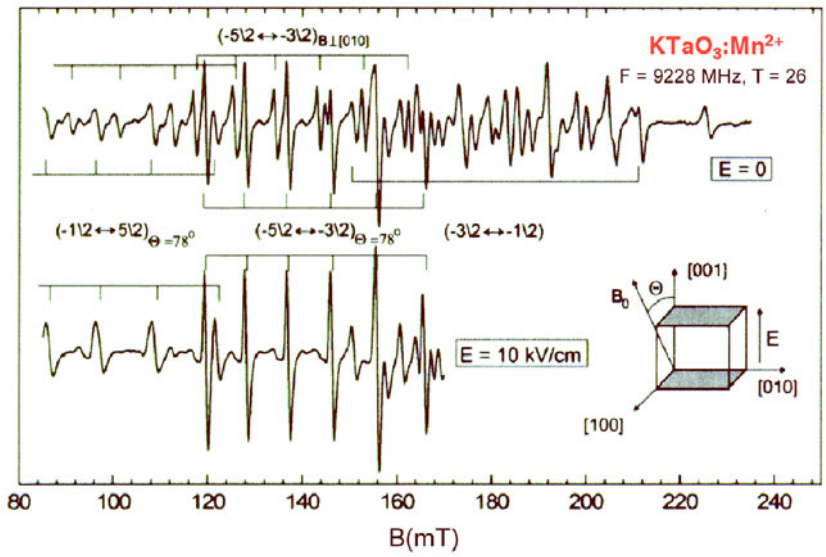

Figure 11. Electric field dependence of the Mn^{2+} ESR spectrum in a Mn-doped $KTaO_3$ crystal (0.01 at.% Mn) measured at 26 K. Also shown is the geometry of the sample configuration with $\theta = 78°$ (after [16]).

decay at a T-dependent rate. The authors studied this decay by monitoring the change in intensity of the ESR lines [16]. They find an exponential decay from which the T-dependence of the relaxation time, τ, is obtained (inset figure 12). The relaxation follows an Arrhenius law, as shown in figure 12, with activation parameters $E = 104(4)$ meV and $1/\tau_0 = 2(2) \times 10^{14}\ s^{-1}$ that agree well with results obtained from the dielectric measurements (see table 1).

From analysis of their ESR results in the dilute limit, i.e., for 0.01 at.% Mn^{2+} where there are no correlations among dipoles, Laguta *et al* [16] deduced the value $\boldsymbol{d} = 1.4\ (2)\ e$Å for the Mn^{2+} dipole moment in $KTaO_3$, and from the symmetry of the ESR spectra they conclude that Mn^{2+} substitutes at the K^+ lattice site. Normally such a substitution will be accommodated by the formation of a near neighbour K vacancy, V_K. However, on the basis of the magnitude of the dipole moment and Lorentz field, the authors argue against such a model. Instead they propose a model whereby the Mn^{2+} ion is displaced by 0.9 Å from the K^+ site along $\langle 001 \rangle$, and charge compensation is achieved by a V_K in a more distant shell. Support for such a model has come from recent first principles calculations as will be discussed later.

While, as shown above, in the dilute limit the dipolar centres introduced by the Fe group substituents in $KTaO_3$ behave as isolated, non-correlated dipolar entities, the situation is expected to be different at higher dopant concentrations. The fact that the correlation length, r_c, for dipolar interactions in $KTaO_3$ is long, especially at low Ts, would indicate that dipolar correlations leading to the formation of clusters of polar nanodomains, or FMRs, should set in at the higher concentrations, as we discussed earlier (section 2). Such correlations produce dipolar glass or relaxor states and will be manifested in both the real and imaginary parts of the dielectric susceptibility. Such states have been observed in Fe-group-doped $KTaO_3$ crystals [16]. Figure 13 shows results for a 0.3 at.% Mn^{2+}-doped crystal [16]. The inset in figure 13 shows the similarity of the $\epsilon'(T)$ response of this sample to a Li^+-doped KT sample that the authors invoke as evidence supporting the existence of a dipolar glass state in Mn-doped $KTaO_3$ at this and presumably higher Mn concentrations, it being known that Li^+-doped

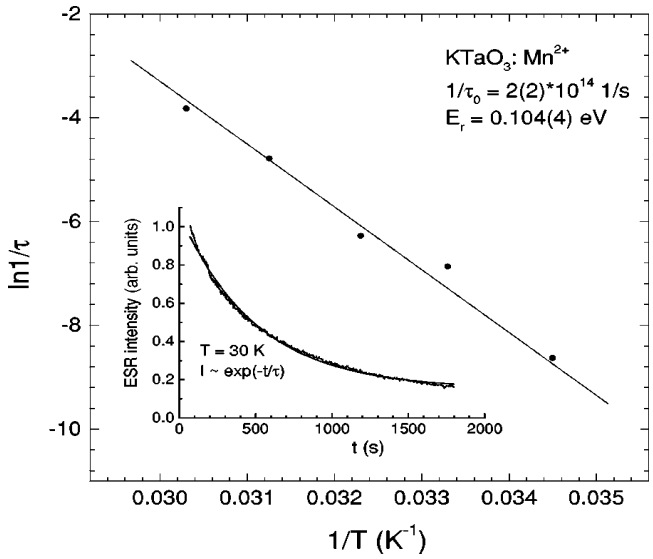

Figure 12. Arrhenius plot of the temperature dependence of the dielectric relaxation time for a Mn-doped $KTaO_3$ crystal (0.01 at.% Mn) deduced from ESR data. The inset shows the decay of the ESR signal intensity after switching off the polarizing electric field (after [16]).

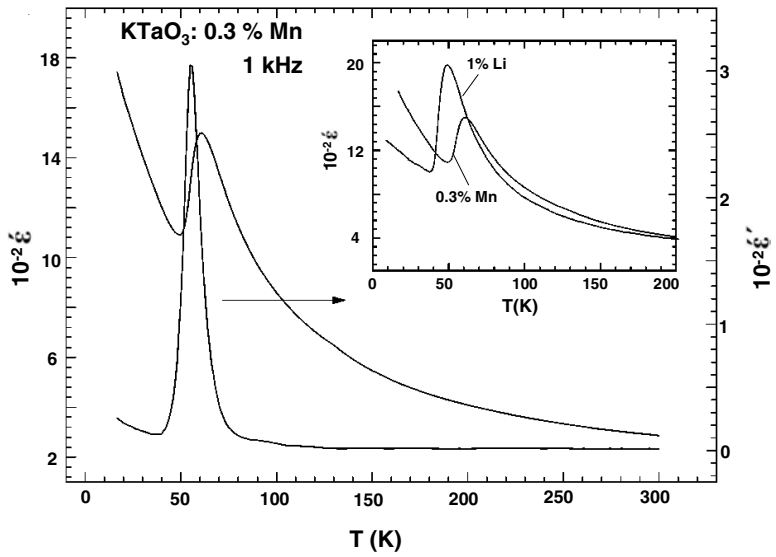

Figure 13. Temperature dependences of the real (ϵ') and imaginary (ϵ'') parts by the dielectric constant of a Mn-doped $KTaO_3$ crystal (0.3 at.% Mn). The inset compares the $\epsilon'(T)$ response of this Mn-doped crystal with that of a Li-doped $KTaO_3$ (1 at.% Li) (after [16]).

KT is a well known dipolar glass system at the 1 at.% Li level. In the presence of correlations, deviations from simple Arrhenius kinetics can be expected, as we shall discuss later (section 4).

The early interpretation that Mn^{2+} and the other transition metal ions in table 1 substitute at the B site and that the relaxing dipolar species is a M^{2+}–V_0 pair defect raised a troubling issue. As can be seen from table 1, the activation energies for the high temperature dipolar relaxations

listed fall in the range ∼100–400 meV. Nowick *et al* [15] noted that these activation energies are much smaller than both

(i) the activation energy for dc ionic conduction in $KTaO_3$ (∼1 eV) which presumably involves some V_0 hopping, and
(ii) the migration energy for V_0 (∼2 eV) obtained from computer simulations.

How can this be if the relaxing defects are M^{2+}–V_0 pairs? Nowick *et al* suggested, that the answer lies in the off-centre configuration of the M^{2+}–V_0 defect. In this configuration the ions surrounding the defect undergo sufficient relaxation to create a lower symmetry configuration than would be the case if the defect pair occupied normal lattice sites. In an applied ac field the defect can then flip among equivalent low-symmetry configurations, a process that should involve smaller motions and, consequently, lower E than for the flipping of the unrelaxed configuration with the defect occupying normal sites. The essential feature of the explanation is that sufficiently large ionic displacements occur around the M^{2+} dopant so as to greatly facilitate the hopping of the pair.

A related argument was also used to provide a plausible explanation for the trend in table 1 that the larger the ionic dopant (which results in larger local distortion of the lattice), the easier the hopping reorientation (or lower E) of the M^{2+}–V_0 pair [23].

The more recent results that the Mn^{2+} ion (and the Fe^{3+} ion [16] and undoubtedly the other ions in table 1) occupies an off-centre position at the K^+ site as well as recent theoretical results, remove the above difficulty as to the magnitude of E. In a recent paper, Leung [24] applied first-principles methods to investigate the energetics, structures and dynamics of Mn^{2+}- and Ca^{2+}-induced dipoles in $KTaO_3$. The calculations employed the Vienna Atomic Simulation Package, which utilizes ultrasoft pseudopotentials. Exchange–correlations were treated in either the local density approximation (LDA) or spin-polarized LDA (SLDA) or in the generalized gradient approximation (GGA). The results show that the Mn^{2+} substitute at the K^+ site, but spontaneously displaces off-centre by 0.81 Å along the ⟨001⟩ direction forming a strong dipole. These results compare very favourably to the above-discussed ESR results of Laguta *et al* [16], analysis of which yielded a displacement of 0.9 Å also along ⟨001⟩. Leung's results also showed that the Mn^{2+} ion moves in the horizontal x–y plane that contains the K^+ site, and the barrier, or E, is predicted to be 180 meV which is in relatively reasonable agreement with the 110 meV deduced from dielectric loss measurements (table 1). On the basis of this result and other considerations, Leung then argues that, in general, metal ion hopping at the A (K^+) site, not oxygen vacancy hopping, is responsible for the small activation energies found in experiments (table 1).

3.3. Lithium (Li) and niobium (Nb) substituted $KTaO_3$

Much work has been done on Li and Nb substitutions in $KTaO_3$ [3, 7, 25]. The early emphasis of this research was aimed at using these substituents to induce a phase transition in the incipient FE $KTaO_3$ by further softening its FE soft mode leading to a long-range ordered FE state. At sufficiently high concentration, Nb substitution does indeed produce the expected softening and a FE state [3, 25–27], but Li substitution actually stiffens $KTaO_3$'s soft mode as shown in figure 14 [28], and the existence of a true phase transition with long-range order in $K_{1-x}Li_xTaO_3$ (or KLT) has remained an uncertain and controversial issue. A variety of studies on KLT have suggested FE behaviour for compositions above 3–4 at.% Li [25, 28–30]. Clearly then, this ferroelectricity is of the order–disorder type and not of the displacive type. For the present purposes, the relevant factor is that for sufficiently low concentrations both Li and Nb substituted KT exhibit dipolar relaxational properties as well as dipolar correlations leading

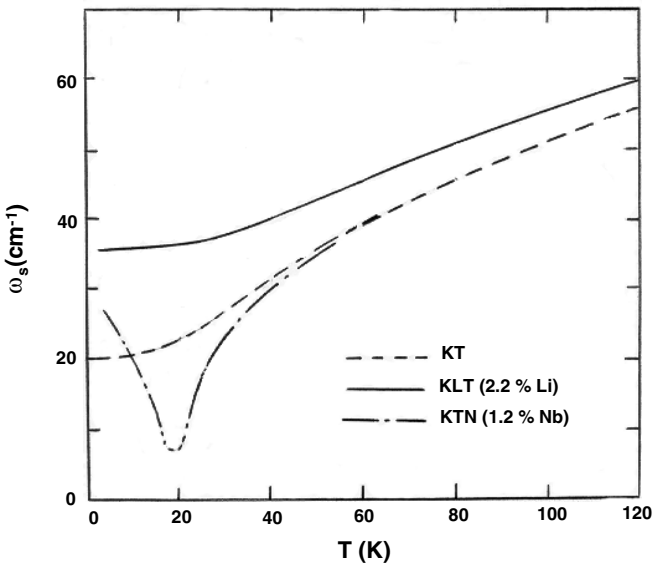

Figure 14. Temperature dependences of the FE soft mode frequencies (ω_s) for $KTaO_3$ and Li-doped $KTaO_3$ (2.2 at.% Li) [28] and for Nb-doped $KTaO_3$ (1.2 at.% Nb) [26].

to the formation of dipolar glass-like relaxor states at low Ts. Some of these properties have been reviewed earlier [3, 7, 25], and in what follows we concentrate on a few issues relevant to the purposes of the present review.

(i) $K_{1-x}Li_xTaO_3$ (KLT).

The substitution of Li^+ for K^+ in KLT raises an immediate issue. The K^+ ion has a radius of 1.3 Å and fits well in the lattice, occupying a centrosymmetric position in the oxygen ion cage that surrounds it in $KTaO_3$. The Li^+ ion, on the other hand, is too small ($r_i = 0.68$ Å), and the oxygen cage is too big for it (figure 15). This is a circumstance that occurs relatively often in solids with the expected consequence that the small ion will shift to an off-centre position. This is expected for Li in KLT, and indeed it was observed early on [31]. The shift, as expected from the lattice symmetry, is in the [100] direction (figure 15) and is quite large (1.2 Å). In this off-centre position, the Li^+ ion has a relatively large dipole moment, which can interact with neighbouring Li dipoles. Additionally, because of the high polarizability of the $KTaO_3$ host, the Li dipole can polarize adjacent unit cells resulting, at relatively small Li concentrations, in polar nanodomains. These are precisely the conditions that lead to dipolar glass and relaxor behaviour. Indeed, this is what is observed experimentally [3, 7, 25]. Figure 16 shows $\epsilon'(T)$ and $\epsilon''(T)$ results for KLT samples with 1.5 and 3.5 at.% Li [32]. Several features in the data deserve comment. Presumably at very low Li concentration (not shown in figure 16(a) or in the inset in figure 13), the $Li^+ \sim$ induced dipoles are sufficiently far apart that there is no $\epsilon'(T)$ anomaly, but clearly by 1 at.% Li a well-defined $\epsilon'(T)$ peak emerges as shown in the inset in figure 13. Results are shown at only 1 kHz, but strong frequency dispersion in both the magnitude of ϵ' and the peak temperature occurs in the region of this peak. This is clearly shown for the sample with 1.5 at.% Li (figure 16(a)). The strong dispersion is also reflected in ϵ'', or ($\tan\delta$) as shown. Additionally, we note the strong enhancement of ϵ' with increasing concentration of dipoles, as expected (cf figure 16(a) and inset, figure 13). This enhancement and the frequency dispersion are further emphasized in the data on a 3.5 at.% Li crystal as

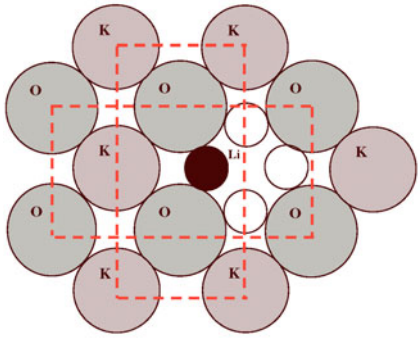

Figure 15. A (100) projection of the ionic positions of Li-doped $KTaO_3$ showing the off-centre position of the Li^+ ion.

shown in figure 16(b) (note the more compressed ϵ' scale compared to figure 16(a)). The appearance of an $\epsilon'(T)$ peak in the response in the absence of a structural phase transition and the dispersion are the signatures of a relaxor state. The relaxation is associated with the jump of Li^+ ions between crystallographically equivalent sites (figure 15). Because corresponding relaxation of the elastic quadrupole moments has been observed in ultrasonic experiments on KLT samples, it has been suggested that the relaxation is most likely by $\pi/2$ (or 90°) flips of the Li positions [32]. We note in passing that a much weaker higher temperature relaxation process seen more clearly in $\epsilon''(T)$ data has been observed for the 1.5 and 3.5 at.% Li samples. This process has been associated with reorientation of a pair of dipoles in head-to-tail configurations [32]. Since such pairs are centrosymmetric, they flip by π (180°) leaving the quadrupole moment invariant, and consequently there is no coupling to acoustic modes, or strain, as verified experimentally [32]. We shall not deal with this process further.

The large increase in the strength of the $\epsilon'(T)$ peak with increasing Li^+ concentration is evidence for increasing cooperative correlation of the reorientation of the Li^+ dipolar nanoregions. As already noted, in the highly polarizable $KTaO_3$ host each Li^+ dipole forms a polar nanoregion at high T whose size is determined by r_c. The higher the Li^+ concentration, the larger the overlap and correlations among these regions. On decreasing T, the sizes of these regions and their correlations increase as r_c increases leading to the strongly enhanced ϵ'. Below T_m the dipolar motion slows down leading to a decrease in ϵ' and in the observed frequency dispersion. Ultimately all dipolar motion freezes at sufficiently low T and the dispersion vanishes as seen in figure 16.

The dipolar relaxation for KLT ($\lesssim$4 at.% Li) is found to obey an Arrhenius law. This is somewhat surprising given the above evidence for some correlation in the dipolar motion. The parameters E and τ_0 vary with compositions, but the variation is quite modest. Typical values are $E = 1140$ K (=98 meV) and $\tau_0 = 1 \times 10^{-13}$ s for a crystal with 1.1 at.% Li [29], and $E = 1280$ K(=110 meV) and $\tau_0 = 1 \times 10^{-14}$ s for a 3.5 at.% Li sample [30].

A feature in the data for the 3.5 at.% Li crystal in figure 16(b) is worth noting. It is seen that on cooling at low frequency the crystal enters the relaxor state at T_m, but on further cooling $\epsilon'(T)$ drops sharply. This drop is believed to be associated with a spontaneous relaxor-to-FE phase transition (marked by T_c in figure 16(b)) seen for this composition and for samples with higher Li concentrations [30, 32]. The transition is first order with thermal hysteresis (figure 16(b)), its T_c appears to be independent of frequency at low frequencies, but its amplitude ($\Delta\epsilon'$) decreases with increasing frequency, and vanishes at high frequencies. A similar phenomenon is seen in a few relaxor FEs in the absence of a biasing dc electric field and in several relaxors

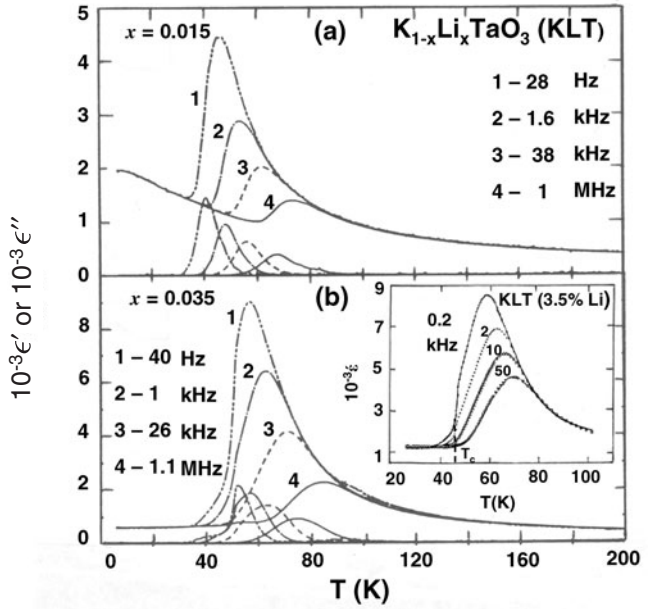

Figure 16. Temperature dependences of the real (ϵ') parts of the dielectric constant of Li-doped $KTaO_3$ crystals: (a) 1.5 at.% Li and (b) 3.5 at.% Li (after [32]). The inset in (b) is the $\epsilon'(T)$ response for another 3.5 at.% Li crystal showing a sharper spontaneous relaxor-to-ferroelectric transition at T_c (adapted from [30]). In each panel the upper set of curves represent ϵ' and the lower set ϵ''.

with bias [3]. The transition is believed to result from continued increasing correlations among the dynamically slowed down nanoregions below T_m resulting in their behaving as collective, macrosized polar regions, i.e., as a FE, on long time scales (low frequencies), but not on short time scales [3].

(ii) $KTa_{1-x}Nb_xO_3$ (KTN).

The case of Nb^{5+} substitution for Ta^{5+} in KTN is not as intuitively obvious. The two ions are identical in size ($r = 0.72$ Å), and it was long assumed, as is reasonable, that the added Nb^{5+} occupies the Ta^{5+} site in the high-temperature cubic phase. The broad features of the temperature–composition phase diagram of the $KTa_{1-x}Nb_xO_3$ (or KTN) system were also known [33]. Over most of the composition range ($\sim 0.1 < x \leqslant 1$) the system exhibits, on cooling, a sequence of three structural phase transitions from paraelectric cubic to FE tetragonal to FE orthorhombic to FE rhombohedral phases as in pure $KNbO_3$. These are equilibrium first-order phase transitions for which the transition temperatures are independent of measuring frequency below microwave frequencies. For compositions $x < 0.1$, the situation has been less clear. There is some evidence for a single phase transition from cubic to rhombohedral symmetry between $x \approx 0.04$ and $x \approx 0.008$ at which point the transition vanishes, and the system remains in the high-temperature cubic phase [3, 25]. However, the evidence was not convincing in the dilute $x < 0.02$ limit, and this uncertainty led to a debate, which is still somewhat ongoing, centred on the question of whether the low-temperature polar phase is a FE or a dipolar glass. The weight of the early evidence was in favour of an FE phase, but now it is generally accepted that the response of dilute ($x < 0.02$) KTN at low temperatures is primarily glass-like resulting from the evolution of the dynamics and ultimate freezing of randomly oriented, thermally activated fluctuations of Nb-based dipolar nanodomains, or so-called microregions [3, 7, 25, 34].

However, there is also evidence from linear birefringence [34] and Raman scattering measurements [35, 36] for some long-range correlations below T_c in the range $x \gtrsim 0.01$ reflected in structural distortions or FE macroregions on a length scale of the wavelength of optical phonons. It has been proposed that these distortions may result from the influence of long-range strain fields which accompany the locally ordered nanodomains, and this led to the suggestion that dilute KTN can be described as a 'cooperative dipole glass' [34]. However, although there is evidence for these long-range FE correlations, we should emphasize that high resolution x-ray diffraction results on a KTN (0.017) sample [37] show no evidence of a structural phase transition (on the length scale of x-ray wavelengths), the structure remaining cubic down to the lowest temperatures, and thereby strengthening the argument for a dipolar glass-like model. For the purposes of this review, we shall restrict the following remarks to the relaxational properties of dilute KTN.

For the dipolar glass explanation to hold, it was first proposed and subsequently confirmed experimentally that in substituting for Ta^{5+}, the Nb^{5+} ion occupies an off-centre position in the lattice in the high-temperature phase [3, 38]. In such a position, the Nb^{5+} would have a large dipole moment. Given that there are several equivalent off-centre positions in the perovskite lattice (the 8 positions along the $\langle 111 \rangle$ direction were believed to be the most likely off-centre positions), the Nb^{5+} was envisioned to hop among these positions. EXAFS results on even a high Nb content sample (9 at.% Nb which exhibits a FE transition at $T_c = 86$ K) showed that the Nb ions are displaced by 0.15 Å to off-centre positions in [111] type directions relative to the Ta, O and K neighbours both above and below T_c [38]. The Ta, on the other hand, remains on centre. This work also revealed that

(i) there is Nb-related disorder both above and below T_c, and
(ii) the size of the Nb off-centre displacement is not affected by the phase transition and does not change over a wide range of temperatures and Nb concentrations.

These observations clearly point to the fact that the Nb displacement is a consequence of short-range interaction of the Nb and its neighbours and not due to a long-range cooperative effect. They are, thus, supportive of a dipolar glass-like model for low Nb concentrations. An off-centre position for the Nb^{5+} ion and its associated polar nanodomain also explains the observed first-order Raman spectrum in KTN samples that do not exhibit a structural phase transition [12].

Figure 17 shows $\epsilon'(T)$ results for KTN samples with 0.9 and 2.0 at.% Nb. The observed frequency dispersion in both ϵ' and ϵ'' (not shown) for the 0.9% sample at 1 bar is the classic relaxor response. At 1 bar the response of the 2% crystal is essentially frequency independent (figure 17 inset), but the application of modest hydrostatic pressure induces a FE-to-relaxor crossover with the strength of the relaxor (R) character increasing with increasing pressure as shown. At sufficiently high pressure the relaxor phase is completely suppressed and the $\epsilon'(T)$ response becomes frequency independent as shown for both compositions in figure 17. While the results in figure 17 (inset) suggest that the FE-to-R crossover in composition at 1 bar is at $x \simeq 0.02$, a more recent study has shown relaxor behaviour in a KTN (3 at.% Nb) sample at 1 bar [30] indicating that there is still considerable uncertainty as to the composition for the crossover. Apparently differences in the degree of crystalline disorder and lattice strain may play a role.

A striking feature in figure 17 is the large sensitivity of the dielectric response to both pressure and applied dc bias. This sensitivity is due to the fact that the anomalies occur in the quantum regime where the characteristic energies are small, and the crystal potentials are strongly influenced by external fields. Thus, e.g., the activation energy for the reorientation of the nanodomains in the 0.9% Nb sample is ~70 K and decreases with pressure [3, 35]. While

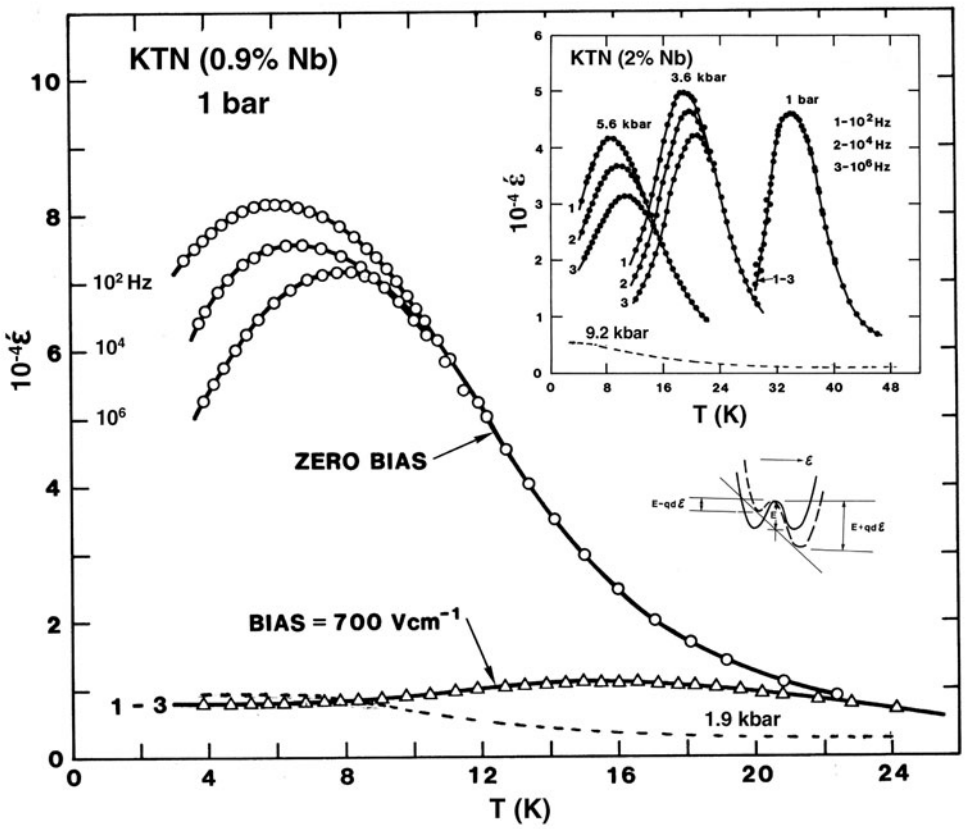

Figure 17. Temperature dependences of the real (ϵ') parts of the dielectric constant for a 0.9 at.% and a 2.0% (inset) Nb-doped $KTaO_3$ crystal at different pressures. Also shown are the quenching effect of a dc biasing electric field and pressure (dashed line) on the $\epsilon'(T)$ response. The second inset depicts the influence of dc bias on the potential for the hopping of the Nb^{5+} ion (after [39]).

both pressure and $\boldsymbol{E}$ field suppress the magnitude of $\epsilon'(T)$ in the region of the peak, pressure suppresses T_m and ultimately causes the vanishing of the relaxor state, whereas $\boldsymbol{E}$ raises T_m and ultimately reinstates the FE state. Both effects are generally understood [3].

The inset in figure 17 illustrates the qualitative picture for the influence of an $\boldsymbol{E}$ field. The solid curve shows a double-well potential that describes the hopping motion of off-centre ions (Nb in the present case) between adjacent equilibrium sites: $\boldsymbol{E}$ is the energy barrier and d is the separation between wells. Application of a biasing field, $\boldsymbol{E}_{bias}$, adds to the potential energy versus distance curve a linear term whose slope is proportional to $\boldsymbol{E}_{bias}$ as shown. The result is modification of the hopping potential making one of the wells deeper, the other shallower and displacing the two minima (dotted curve). This makes hopping from the deeper well more difficult, requiring more thermal energy, i.e., higher T_m. The $\boldsymbol{E}_{bias}$ also causes alignment of the polar nanodomains with the field, and, for sufficiently large field and high enough concentration of large domains, can reinforce a FE state. Such a field-induced state has been observed in relaxors [3], but does not appear to have been pursued in KTN. The large suppression of the magnitude of ϵ' with $\boldsymbol{E}_{bias}$ is due to the reduction of the polarizability

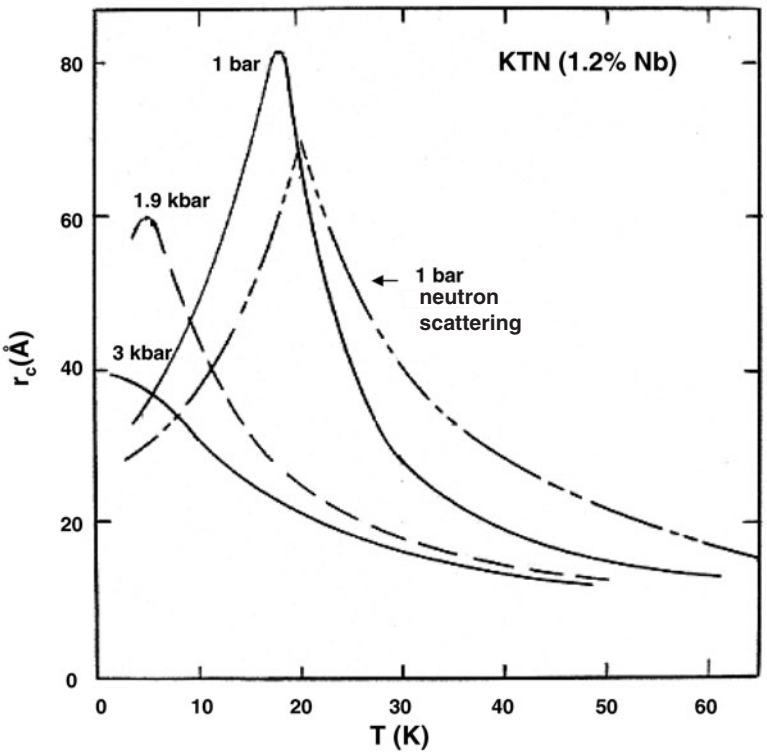

Figure 18. Temperature dependence of the correlation length for dipolar interactions in Nb-doped $KTaO_3$ (1.2 at.% Nb) determined from inelastic neutron scattering at 1 bar (dashed curve, [27]) and dielectric measurements at several pressures (after Samara, unpublished).

associated with the alignment of domains and the concomitant stiffening of the soft mode of the host lattice with $\boldsymbol{E}_{bias}$.

3.4. Pressure-induced FE-to-R crossover

The usual approach for inducing relaxor behaviour has been varying the degree of crystalline disorder by chemical substitution. However, this approach introduces complications such as added compositional fluctuations (or randomness), lattice defects, lattice strains and changed interatomic forces. These complications have made it difficult both to interpret and understand experimental data and to determine the mechanism for the FE-to-R crossover. The alternate approach illustrated above for KTN (0.02) is intrinsically more direct. By applying pressure to a sample of fixed composition one changes only the balance between competing short- and long-range forces making interpretation of experimental data simpler. The pressure-induced FE-to-R crossover has been shown to be a general feature of soft-mode FEs with dipolar impurities or polar nanodomains [3]. Other examples will be shown in section 4. This phenomenon has been attributed to the unique pressure dependence of the soft-mode frequency, ω_s, which controls the polarizability of the lattice and thereby ϵ' and the correlation length for dipolar interactions, r_c.

Foussadier and Fontana [27] determined $r_c(T)$ at 1 bar for a KTN (0.012) crystal from inelastic neutron measurements of the soft TO_1 phonon branch as follows. The dispersion of the soft TO_1 phonon frequency Ω with wavevector $\boldsymbol{q}$ in the small $\boldsymbol{q}$ regime can be written

as [27]

$$\Omega_q^2 = \omega_0 + D^2 q^2, \tag{16}$$

where ω_0 is the frequency at $\boldsymbol{q} = 0$, and D is a parameter that describes the shape of the dispersion curve. Equation (16) leads to the definition of r_c as

$$r_c = \left(\frac{D}{2\pi\omega_0}\right) a_0, \tag{17}$$

where a_0 is the lattice parameter. A replot of the authors' results is shown in figure 18.

Because $r_c \sim 1/\omega_0 (= \omega_s)$, r_c can be determined from the $\epsilon'(T)$ response, namely $r_c(T) \sim \sqrt{\epsilon'(T)}$. Such a determination gives the relative change of r_c with T and not the absolute value of r_c. However, the $r_c(T)$ deduced from the neutron results can be used to normalize the dielectrically deduced $r_c(T)$. This is done in figure 18, which also shows $r_c(T)$ at several pressures for the KTN (0.02). The normalization was done at $T = 100$ K where r_c should be essentially independent of Nb content. The very large suppression of r_c with pressure is clearly evident.

To explain the pressure-induced FE-to-R crossover for a sample of fixed composition, we envision each dipole inducing polarization (or dipoles) in adjoining unit cells and forming a dynamic polarization 'cloud' whose extent is determined by the correlation length for dipolar fluctuations, r_c. At high temperatures r_c is small and the polarization clouds are effectively polar (FE) nanodomains. With decreasing T at 1 bar and low pressures (<3 kbar in figure 17 inset), the rapidly increasing r_c couples these nanodomains into rapidly growing polar clusters and increases their Coulombic interactions. Ultimately, these clusters percolate (or permeate) the whole sample and precipitate a static, cooperative long-range ordered FE state at $T \leqslant T_c$. At sufficiently high pressure (>3 kbar in figure 17 inset) on the other hand, the clusters increase in size on decreasing T in the PE phase, but do not become large enough to permeate the whole sample (or grains) and precipitate a FE transition. Rather, the clusters exhibit a dynamic 'slowing down' of their fluctuations at $T \leqslant T_m$ leading to the observed relaxor behaviour. Because r_c decreases continuously with increasing pressure, the polar clusters become smaller with increasing pressure, a fact that accounts for the observed increase in the frequency dispersion and suppression of the dielectric anomaly. It is thus seen that the FE-to-R crossover results simply from the large decrease in r_c with pressure, a unique property of soft FE mode materials. Ultimately, the nanodomains become so small that there are no correlations among them and they contribute little to the polarizability of the lattice. The response is then very similar to that of pure $KTaO_3$. This is the case for the 9.2 kbar results in figure 17 inset.

At sufficiently low dopant concentration and in the absence of dipolar correlations, the dynamics of the hopping motion of dipolar entities obeys Arrhenius T dependence (equation (5)). However, at higher concentrations where dipolar correlations come into play, deviations from equation (5) are generally observed. In such cases the response is often adequately described in terms of the Vogel–Fulcher expression

$$1/\tau = (1/\tau_0) \exp[-E/k(T - T_0)], \tag{18}$$

where the parameters are given the following physical interpretation: $(1/\tau_0)$ is the attempt frequency which is related to the cut-off frequency of the distribution of relaxation times, E is the energy barrier to dipole reorientation and T_0 is a reference temperature where all relaxation times diverge (and where the distribution of relaxation times, τ, becomes infinitely broad). T_0 can be viewed as the 'static' dipolar freezing temperature for the relaxation process. Combining dielectric and Raman data, it has been shown that the dynamics of dipolar hoping in KTN (0.009) obeys equation (18) over nine decades of frequency [3, 35].

3.5. Calcium-doped $SrTiO_3$

Relaxor character has been observed in the system $Sr_{1-x}Ca_xTiO_3$, SCT, in the limit of small x. Because the Sr^{2+} and Ca^{2+} ions have the same valence, intuitively, Ca^{2+} might be expected to substitute for Sr^{2+} at the A site in the ABO_3 perovskite lattice. However, the evidence is clear that the Ca^{2+} dopant in $SrTiO_3$ is dipolar. This evidence, supported by the existence of Ca-induced nanodomains at $T > T_m$, has come from dielectric, Raman scattering and second-harmonic generation of light measurements on SCT (0.007) by Kleemann and collaborators [40, 41]. Ca^{2+}'s ionic radius (0.99 Å) is considerably smaller than that of Sr^{2+} (1.12 Å), making it possible for the Ca^{2+} to occupy an off-centre position at the Sr^{2+} site thereby producing random electric field and strain coupling to the polarization. Alternatively, some of the Ca^{2+} may substitute at the Ti^{4+} site. In this case, analogy with ESR results on Mn^{2+} in $SrTiO_3$ suggests that the Ca^{2+} impurity would sit at an off-centre position at the Ti^{4+} site [42]. To preserve charge neutrality, this substitution has to be accommodated by the formation of an oxygen vacancy (V_0). The dipolar impurity would then be the Ca_{Ti}:V_0 pair defect. Although it is not at present known which of these two alternatives is dominant, as we noted earlier recent theoretical results on $KTaO_3$ suggest that in general metal ion impurity hopping at the A site, and not (dopant: V_0) pair hopping, is responsible for the small activation energies found in experiments [24].

Kleemann *et al*'s [41] studies of SCT (0.007) have suggested that this composition exhibits an inhomogeneous polar, low-temperature phase with evidence for ordering at two length scales:

(1) local ordering associated with individual nanodomains leading to the relaxor character of the response, and
(2) ordering on a longer length scale revealed by the analysis of the field-dependent macroscopic polarization via linear birefringence measurements and which suggests the presence of large random-field correlated domains.

This situation is thus qualitatively similar to that for dilute KTN as described above. Again, as in the case of KTN, there is no evidence of a structured phase transition at $\leqslant T_m$.

Figure 19 shows the relaxor-like $\epsilon'(T)$ of SCT (0.007) at 1 bar and elevated pressures [43]. A remarkable feature of these results is the extremely large influence of pressure on T_m, an effect nearly an order of magnitude larger than that for KTN (0.02) in figure 17. In this case T_m decreases by $\sim$35 K kbar^{-1}, and the relaxor state and frequency dispersion in ϵ' are completely suppressed by 0.5 kb. It is estimated that $T_m \approx 0$ K at this pressure, and, as shown in figure 19, the 0.5 kbar $\epsilon'(T)$ response is close to that of pure $SrTiO_3$ at 1 bar indicating that dipolar correlations in SCT (0.007) have become very weak at this pressure.

Very modest dc biasing electric fields have been shown to strongly influence the relaxational response of SCT (0.007) [40, 43]. Figure 20 shows these effects at 0.1 and 0.2 kbar [43]. The large suppression of the peak amplitude ϵ'_{max} and the shift of T_m to higher temperatures are the expected behaviours in the quantum regime, as discussed for KTN in section 3.3 above. The application of a biasing field stabilizes the local potential of a dipolar entity making one of its potential minima deeper and the other shallower (insert in figure 17) thereby raising the transition temperature. The SCT (0.007) results give a quantitative measure of this effect [43]. Additionally, the field aligns and clamps the polarization of the sample reducing its small signal ac susceptibility, i.e., suppressing ϵ'. These effects are well known from Landau free energy theory, which predicts that T_m increases with field strength as $E^{2/3}$. The 1 bar and high-pressure data confirm this prediction for $E > 50$ V cm^{-1} [40, 43]. Another feature to note is the fact that these very large biasing field effects occur only in the quantum regime. They vanish above $\sim$30 K as shown in figure 20 and seen in the 1 bar data.

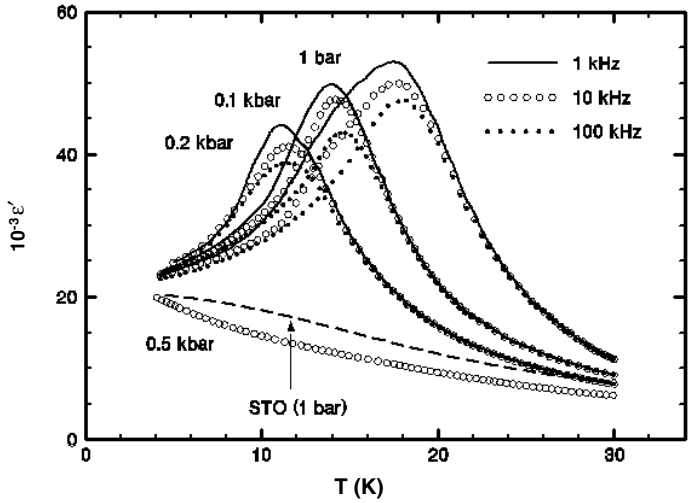

Figure 19. The dielectric $\epsilon'(T)$ response of a Ca-doped $SrTiO_3$ crystal (0.7 at.% Ca) at different pressures showing the frequency dispersion, which vanishes at 0.5 kbar. Also shown for comparison in the frequency-independent response of pure $SrTiO_3$ (STO) at 1 bar (after [43]).

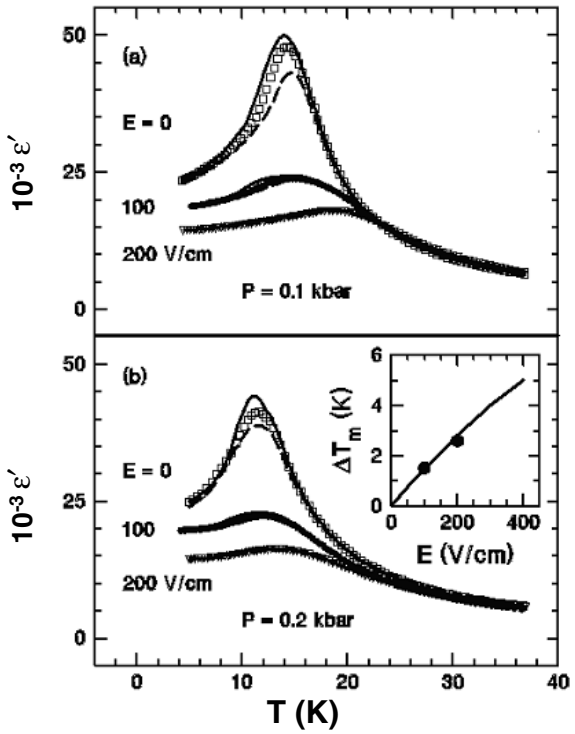

Figure 20. The influence of dc bias on the $\epsilon'(T)$ response of Ca-doped $SrTiO_3$ crystal (0.7 at.% Ca) at 0.1 and 0.2 kbar. The inset in (b) shows the shift of the glass transition temperature T_m with field for SCT (0.007) at 1 bar (solid curve, [40]) and at 0.2 kbar (solid circles) (after [43]).

In the case of relaxors, additional biasing field effects can be expected and are observed. Cooling a relaxor in the presence of a dc field aligns its polar nanodomains increasing their sizes and correlations, effectively cancelling the influence of random fields and reducing the frequency dispersion in the relaxor state. At sufficiently high fields, which are still very modest in the quantum regime, the domains can become sufficiently large so as to percolate the whole sample and lead to the onset of long-range order and a normal FE transition. This is a field-induced nano-to-macrodomain transition. Evidence for such a transition in relaxors has come from dielectric response and TEM measurements [3].

Evidence for these effects can be seen in the SCT (0.007) pressure results (figure 20). The relaxor nature of the response at low bias is evident. The dispersion is essentially gone at the very modest field of $\sim$300 V cm^{-1}. Taking $\Delta T_f (= T_m$ at 10^6 Hz–T_m at 10^2 Hz) as a measure of the relaxational strength, it is found that ΔT_f decreases from 1.8 K at 0 V cm^{-1} to 0 K by 300 V cm^{-1} [43]. The vanishing of the dispersion in T_m at high bias is a reflection of the transition acquiring normal FE character, as expected [3].

Finally, we note the large pressure and bias field effect on both SCT (0.007) and dilute KTN are a reflection of the fact that the 'transitions' in these materials occur in the quantum regime where the characteristic energies are small making them very sensitive to external fields, as observed. The much larger effects in the case of SCT (0.007) are especially remarkable and reflect a more delicate balance between competing short-range and Coulomb forces in the case of SCT (0.007) as compared with KTN (0.02).

4. The strong high temperature ABO_3 relaxors

In section 3 we dealt with the relaxational properties of the simple, doped incipient FEs $KTaO_3$ and $SrTiO_3$. While these systems have been very fruitful from a physics point of view, the relaxational effects are relatively weak and occur at low temperatures. Much stronger relaxational effects and at much higher temperatures are prominent in disordered ABO_3 FEs with mixed compositions. These relaxors possess very large dielectric constants, attractive for capacitors, exceptionally large electrostrictive coefficients, important for actuators and micropositioners, and large electro-optic constants, useful for information storage, shutters and optical modulators. Because of these remarkable properties and their applications, relaxors are one of the most active current research areas of ferroelectricity [3]. The properties of prototypical examples of these strong relaxors have been recently reviewed [3], and here we restrict ourselves to a few general features and recent results on selected materials. These include the $PbMg_{1/3}Nb_{2/3}O$ or (PMN) family and the lanthanum-substituted $PbZr_{1-x}Ti_xO_3$ (PLZT) family. They have been the most studied and best understood mixed ABO_3 relaxors. We start with some general remarks.

4.1. The physical picture and dielectric response

In reflecting on the occurrence of relaxor behaviour in perovskites, there appear to be three essential ingredients:

(1) the existence of lattice disorder,
(2) evidence for the existence of polar nanodomains at temperatures much higher than T_m, and
(3) these domains exist as islands in a highly polarizable (soft mode) host lattice.

The first ingredient can be taken for granted since relaxor behaviour in these materials does not occur in the absence of disorder. The third ingredient is also an experimental fact in that relaxor

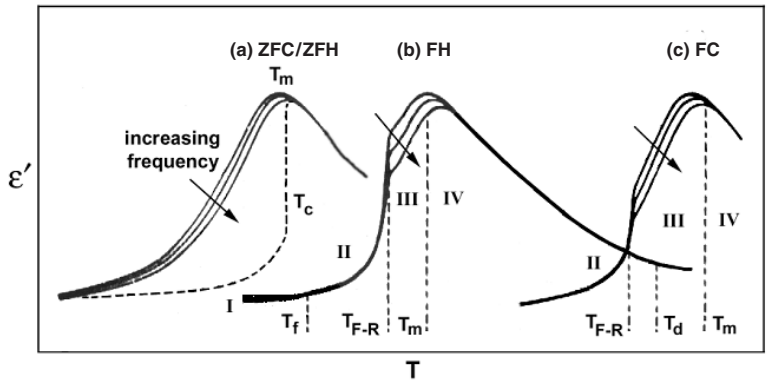

Figure 21. The various dielectric responses of relaxors both without and with electric field bias as discussed in the text. Response (b) defines all the various characteristic 'transition' temperatures of a relaxor.

behaviour occurs in ABO_3 oxides with very large dielectric constants. The second ingredient is manifested in many experimental observations common to all perovskite relaxors, as we shall discuss later.

The physical picture that has emerged for the strong relaxors is not unlike that for the simple weak relaxors in section 3. Chemical substitution and lattice defects introduce dipolar entities in mixed ABO_3 perovskites [3]. At very high temperatures, thermal fluctuations are so large that there are no well-defined dipole moments. However, on cooling, the presence of these dipolar entities manifests itself as small polar nanodomains below the so-called Burns temperature, T_d. These domains grow as the correlation length, r_c, increases with decreasing T, and ultimately, one of two things happen. If the domains become large enough (macrodomains) so as to percolate (or permeate) the whole sample, then the sample will undergo a static, cooperative FE phase transition at T_c. On the other hand, if the nanodomains grow with decreasing T but do not become large enough or percolate the sample, then they will ultimately exhibit a dynamic slowing down of their fluctuations at $T \leqslant T_m$ leading to an isotropic relaxor state with random orientation of the polar domains.

The above describes the situation in the absence of a biasing electric field. Cooling in the presence of a biasing field, however, aligns the domains and increases their correlation length, effectively cancelling the influence of the random fields. For sufficiently large $\boldsymbol{E}_{bias}$ the domains become large leading to the onset of long-range FE order. This is a field-induced nano-to-macrodomain transition. This transition occurs spontaneously in some cases in the absence of bias as we have seen for KLT (3.5 at.% Li) in section 3.3 and as will be shown for PLZTs, in section 4.4. Evidence for the nano-to-macrodomain transition in relaxors can be inferred, as we shall see, from the dielectric response and can often be seen in TEM images and from scattering data [44]. Its occurrence is determined by a delicate balance among $\boldsymbol{E}_{bias}$, thermal fluctuations and the strength of dipolar correlations.

Much insight about the physics of strong relaxors has been gained from measurements in the presence dc bias. Such measurements lead to distinctive behaviour as shown for $\epsilon'(T)$ in figure 21. Figure 21(a) is the signature of a relaxor in the absence of bias. The same relaxational response is observed under both zero-field cooling (ZFC) and zero-field heating (ZFH) conditions. The dashed curve depicts the field-induced, frequency-independent FE response for sufficiently large $\boldsymbol{E}_{bias}$ which stabilizes the FE phase at low temperatures. Figures 21(b) and (c) show the responses for intermediate biases. For field heating (FH) conditions after

ZFC, the response has four regions (figure 21(b)). Region I is a dispersive region consisting of frozen-in, randomly oriented nanodomains. Below T_f (a freezing temperature) there is not enough thermal energy to unfreeze and align the domains with the field. However, at $T \geqslant T_f$ (region II) the nanodomains align and grow, forming macrodomains. This is a dispersion free FE region. On further heating, a temperature, T_{F-R}, is reached above which thermal fluctuations become sufficiently large so as to break the ordering tendency of the intermediate strength biasing field. As a result, the macrodomains break into randomly oriented, slowed down nanodomains, i.e., a dispersive relaxor state (region III). Finally, above T_m the sample enters the PE state (region IV) where the nanodomains undergo rapid thermal fluctuations. Also shown in figure 21(b) is the fourth characteristic temperature, the Burns temperature, T_d, where nanodomains first nucleate. It occurs, as already noted, at $T \gg T_m$.

Figure 21(c) shows the response of the sample under field cooling (FC) conditions for intermediate strength fields. Regions IV and III are similar to those in figure 21(b). However, at $T \leqslant T_{F-R}$ the behaviour is different. Here the field aligns and grows the nanodomains into macrodomains (a FE state). Once aligned, the macrodomains remain aligned and stable down to the lowest temperature in the presence of the field. Thus region I is absent in this case.

4.2. Evidence for the existence of polar nanodomains above T_m

Evidence for the existence of polar nanodomains well above T_m has come from high resolution TEM which also showed the growth of these domains with decreasing T [3]. The evidence is also prominently reflected in certain properties of these systems. To provide the context, recall that for relaxors in the absence of electrical bias there are random + and − fluctuations of the dipolar polarization so that $\sum P_d = 0$, i.e., there is no measurable remanent polarization. However, $\sum P_d^2 \neq 0$, and we then expect the existence of these polar domains to be manifested in properties which depend on P^2, e.g., eletrostriction which is reflected in the thermal expansion and the quadratic electro-optic effect, which is reflected in the refractive index, or birefringence. Indeed, both of these properties have provided quantitative measures of this polarization for the strong relaxors.

Specifically, for a cubic perovskite it can be easily shown that the axial thermal strain, x_{11}, is given by [3, 45]

$$x_{11} = \frac{\ell_T - \ell_0}{\ell_0} = \alpha(T - T_0^*) + (Q_{11} + 2Q_{12})P_d^2, \tag{19}$$

where ℓ_T is the sample length at temperature T, ℓ_0 is the reference length at the reference temperature T_0^*, α is the linear coefficient of thermal expansion and Q_{11} and Q_{12} are electrostrictive coefficients. Thus, in the presence of dipolar polarization, there are two contributions to the total thermal strain; the usual linear expansion (the first term on the right-hand side of equation (19)) and the contribution due to electrostriction (the second term in equation (19)). This latter contribution vanishes above T_d where $P_d \to 0$. Figure 22(a) shows an example of the strain versus T for a typical strong relaxor, PMN [45].

The manifestation of the presence of polar nanodomains in strong relaxors in terms of the electro-optic effect was first demonstrated by Burns and Dacol [46] in measurements of the T dependence of the refractive index, n. For a normal ABO_3 FE crystal, starting in the high-temperature PE phase, n decreases linearly with decreasing T down to T_c at which point n deviates from linearity. The deviation is proportional to the square of the polarization and increases as the polarization evolves with decreasing T. If the FE transition is first order, then there is a discontinuity in n at T_c followed by the expected deviation. This qualitative picture is representative of the behaviour of many perovskite FEs. However, in the case of relaxors, Burns and Dacol observed deviations from linear $n(T)$ well above T_m. In the case of PMN

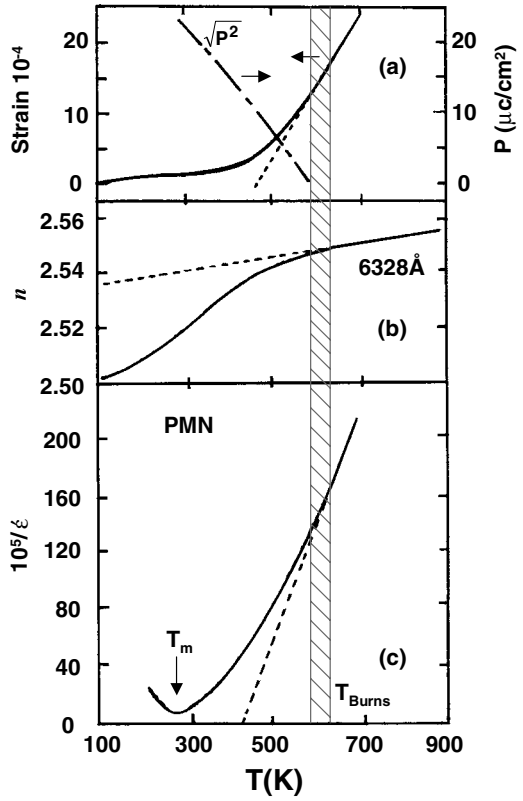

Figure 22. Temperature dependences of the linear thermal expansion, $\Delta\ell/\ell$ [45], refractive index, n [46] and reciprocal dielectric constant, $1/\epsilon'$ (Samara, unpublished) for PNM showing deviations from linear response at a temperature (T_{Burns}) much higher than the peak (T_m) in the dielectric susceptibility.

(figure 22(b)) these deviations became discernible on cooling at $T = 620$ K, or about 350 K above T_m, a remarkably large T range. These deviations can be quantitatively described by the relationship [3, 46]

$$\Delta n = \frac{\Delta n_{11} + 2\Delta n_{\perp}}{3} = \frac{{n^o}^2}{2}\left[\frac{g_{33} + 2g_{13}}{3}\right]P_d^2 \tag{20}$$

where the Δn's are the changes in the parallel and perpendicular components of n, n^o is the index in the absence of polarization (P_d), represented by the dashed straight line in figure 22(b), and the gs are the electro-optic coefficients. The temperature at the onset of the deviation from linear $n(T)$, 620 K in the case of PNM, is the Burns temperature, T_d in our notation. Above this temperature, thermal fluctuations are so large that there are no well-defined dipoles or dipolar domains. These domains nucleate at T_d and grow on lowering T. Diffuse scattering and HRTEM results indicate that in PMN these domains grow from 2 to 3 nm in size above 400 K to ∼10 nm at ∼160 K ($T_m \cong 230$ K) [3]. Thus, they are much smaller than typical FE domains, which are orders of magnitude larger. The small size of these nanodomains explains why they cannot be detected by diffraction measurements, the bulk structures of PNM and most strong mixed ABO_3 relaxors remaining cubic to both x-ray and neutron probes and to long wavelength photons down to the lowest temperatures.

Evidence for the existence of polar nanodomains well above T_m in strong relaxors has also been deduced from the T dependence of the susceptibility. As noted earlier, it is well established that $\epsilon'(T)$ in the high temperature, cubic PE phase of ABO_3 FEs follows the Curie–Weiss law $\epsilon' = C/(T-\theta)$, where θ is the Curie–Weiss temperature, over a wide temperature range. However, $\epsilon'(T)$ of relaxors shows large deviations from this law for $T > T_m$. This is shown in figure 22(c) for PNM. The results show that a linear $1/\epsilon'(T)$ response obtains only above ~625 K. An important point is that this is the same temperature, T_d, where deviations from linear $n(T)$ and $x(T)$ occur as shown (figure 22). Thus, deviation from Curie–Weiss response sets in upon the nucleation of polar nanodomains, and this deviation increases with decreasing T as the size of the domains and their correlations increase. This deviation can be described by the power law expression [3]

$$\epsilon' - \epsilon'_\infty = C(T-\theta)^{-\gamma} \tag{21}$$

where ϵ'_∞ is the high frequency dielectric constant, and $\gamma > 1$. However, it has been generally observed that no single value of γ is found which uniquely describes the $\epsilon'(T)$ dependence for relaxors.

Deviations from Curie–Weiss behaviour are commonly observed in the temperature dependence of the magnetic susceptibility, χ, of spin glasses [47] above the freezing temperature of spin fluctuations, T_f (which corresponds to T_d for relaxors). For an ideal superparamagnet, i.e., for non-interacting paramagnetic particles or clusters, $\chi(T)$ exhibits Curie–Weiss behaviour. This behaviour is achieved in spin glasses for temperatures $\gg T_f$. At lower temperatures, deviation from the Curie–Weiss law is attributed to strong local magnetic correlations [47] and the onset of local (spin-glass) order below T_f. Sherrington and Kirkpatrick [48] developed a model, which relates $\chi(T)$ below T_f to the local order parameter q. The expression is

$$\chi = \frac{C[1-q(T)]}{T-\theta[1-q(T)]} \tag{22}$$

where it is seen that q is a function of temperature. Clearly q and its temperature dependence can be evaluated from $\chi(T)$ data and the values of C and θ determined from the high-temperature $\chi(T)$ response above T_f which follows a Curie–Weiss law. In this high-temperature regime $q \to 0$ and equation (22) simply reduces to a Curie–Weiss form. Equation (22) can be thought of as a modified Curie–Weiss law where both C and θ are functions of temperature.

If we presume, as we believe to be the case, that the deviation from Curie–Weiss behaviour in PNM and other relaxors is due to correlations among local nanodomains, then we may evoke equation (22) to treat the high-temperature dielectric response of relaxors. Indeed this equation has been shown to provide a satisfactory description of the $\chi(T)$ response of relaxors [3, 49]. As expected, $q \to 0$ above, e.g., ~625 K for PMN, and it increases with decreasing temperature below T_d because of increased dipolar correlations [49]. In such a case the local order parameter due to correlations between neighbouring polar domains of polarization P_i and P_j is $q = \langle P_i P_j \rangle^{1/2}$.

4.3. Lead magnesium niobate, $PbMg_{1/3}Nb_{2/3}O_3$ (PMN), and related relaxors

As a well-defined chemical compound, PNM is perhaps the simplest of the strong ABO_3 relaxors, but its physics, and in particular the nature of its low T ground state, has been and remains challenging despite very extensive research [3, 45, 50, 51]. The disorder that is believed to be responsible for the relaxational properties of PMN, is brought about by differences in valence (5+ versus 2+), ionic radii (0.64 versus 0.72 Å) and electronegativities (1.6 versus 1.2 on the Pauling scale) between Nb^{5+} and Mg^{2+} ions on the B site which introduce charge

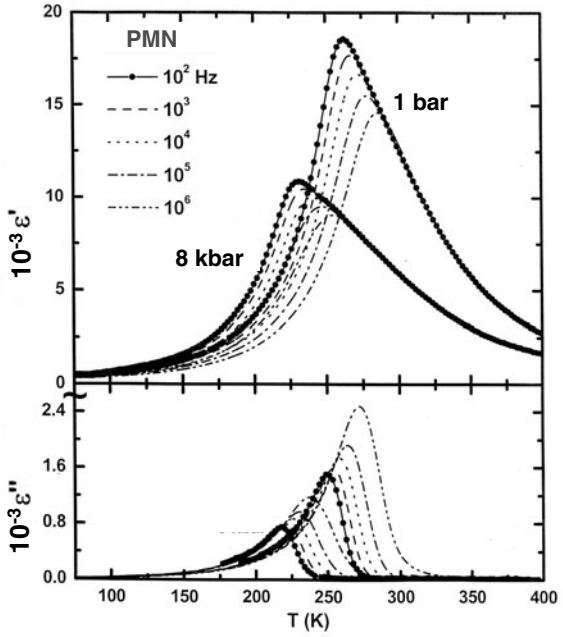

Figure 23. Temperature dependences of the (ϵ') and imaginary (ϵ'') parts of the dielectric constant of PMN showing the strong frequency dispersion. Also shown is the influence of pressure (8 kbar) on these responses (after [3]).

fluctuations and local order. This order is the origin of the nanodomains whose existence in PMN is now well established, as discussed above.

Figure 23 shows the relaxational dielectric response of PMN at 1 bar and elevated pressure. The shift of T_m to lower temperature and the suppression of the dielectric anomalies with pressure are the signatures of ABO_3 relaxors as discussed in section 3, and they can be understood in terms of soft mode and relaxor theory [3]. The application of dc bias results in significant changes in the dielectric response and has provided important insights into the physics [50, 51]. Specifically, cooling in the presence of a bias field (for fields above a threshold field of $\boldsymbol{E}_{th} \cong 1.8$ kV cm^{-1}) causes PMN to first enter the relaxor phase at $T \leqslant T_m$, and on further cooling it transforms to a long-range ordered, rhombohedral FE state at T_c below which the dispersion in $\epsilon'(T)$ vanishes. This behaviour is akin to that observed in KLT (3.5% Li) discussed in section 3.3. At $\boldsymbol{E}_{th}$, $T_c = 213$ K, and it increases with increasing $\boldsymbol{E}$ as expected for a FE. Ye [51] has reported the $\boldsymbol{E}$ versus T phase diagram for PNM at fields up to 10 kV cm^{-1}). Presumably the random electric and strain fields associated with the polar domains suppress the FE transition in the absence of bias [3, 51], and $\boldsymbol{E}_{th}$ is then the field strength required to overcome the influence of the random fields and induce the transition. We should hasten to note, however, that a R-to-FE transition occurs spontaneously in some relaxors (e.g., KLT and PLZT) even in zero bias over limited composition and temperature ranges [3].

Lead zinc niobate, $PbZn_{1/3}Nb_{2/3}O$ (PZN) is isomorphous with PMN and exhibits full relaxor properties analogous to the latter except for higher characteristic temperatures [52], e.g., $T_m \cong 410$ K versus ∼270 K at 10^4 Hz. The symmetry breaking compositional and structural disorder due to differences between the Nb^{5+} and Zn^{2+} ions is responsible for the relaxor character of PZN. Compared with PMN, relatively little research has been done

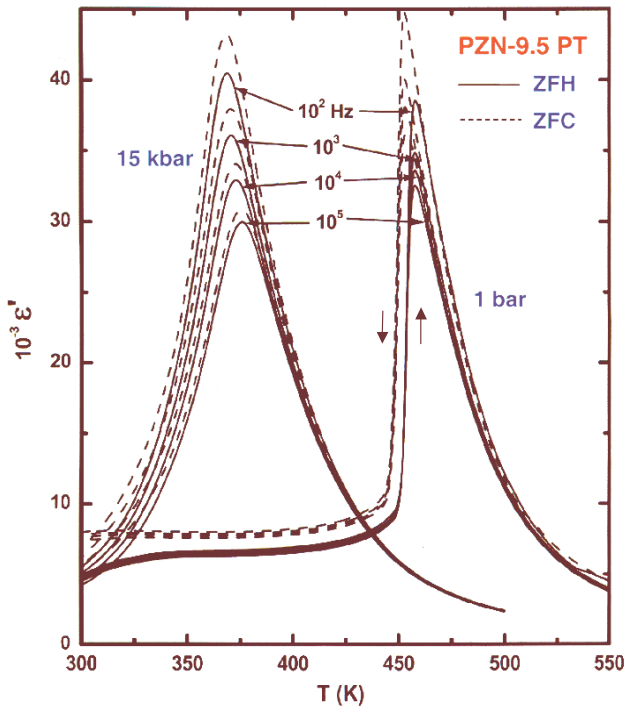

Figure 24. Temperature dependence of the real part (ϵ') of the dielectric constant of PZN–9.5 PT at 1 bar and 15 kbar showing the pressure-induced FE-to-relaxor crossover. Data are shown on both heating (H) and cooling (C) in the absence of dc bias, i.e., in zero field (ZF) (after [55]).

on PZN, a recognition of the expectation that the behaviours of the two crystals should be qualitatively similar. However, mixed single crystals of PZN and $PbTiO_3$ (PT), or $PZN_{1-x}PT_x$ have been attracting a great deal of recent interest because of their ultrahigh piezoelectric and electromechanical coupling coefficients for compositions near the morphotropic phase boundary ($x \cong 0.09$–0.095) [53]. These properties have the potential of greatly advancing transducer/actuator technology. While PZN is a characteristic relaxor, PT is the classic soft FE mode FE which transforms on cooling from the cubic PE phase to a tetragonal ($P4\,mm$) FE phase at $T_c = 760$ K. Its addition to PZN, even at the $0.05 \leqslant x \leqslant 0.15$ level, imparts FE character to the mixed crystals. On cooling, such crystals transform from the cubic PE phase to a tetragonal FE phase and then to a rhombohedral FE phase. We should also note that mixed single crystals of PMN and PT have been grown and studied. They behave qualitatively similar to PZN/PT but retain their relaxor character to higher PT concentrations (~30 mol%) [54].

The dielectric response at 1 bar of a crystal PZN/PT with $x = 9.5$ mol% PT is shown in figure 24 for both ZFH and ZFC [55]. The most prominent feature is the large anomaly at the cubic–tetragonal FE transition at ~460 K. The transformation is remarkably sharp for a complex, compositionally disordered mixed crystal and is thermodynamically first order as evidenced by the ~5 K thermal hysteresis. The transition temperature, T_c, taken as corresponding to the peak in $\epsilon'(T)$ is independent of frequency. The relatively weak frequency dispersion in $\epsilon'(T)$ at and above the peak is characteristic of many mixed perovskite FEs. At

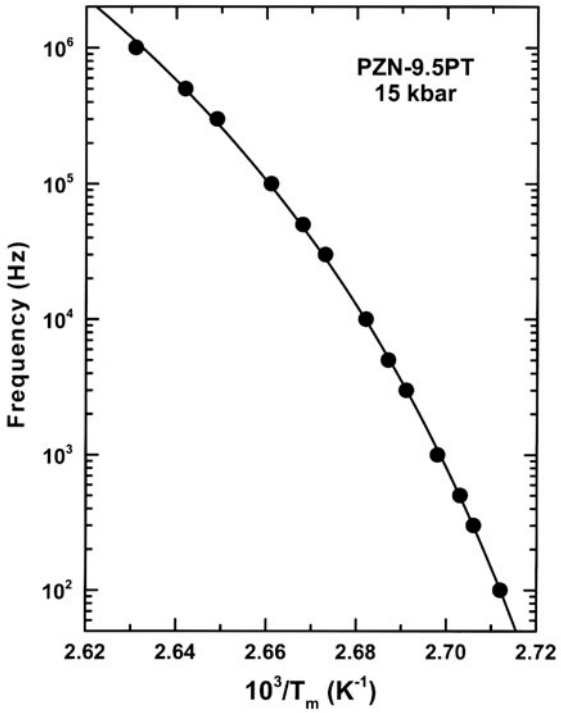

Figure 25. Temperature dependence of the dipolar relaxation frequency for PZN–9.5 PT at 15 kbar (after [55]).

lower temperatures than shown in figure 24 the sample transforms from the tetragonal to a rhombohedral FE phase. The signature of this transformation is a step in $\epsilon'(T)$, and the transition is first order with a large thermal hysteresis [55].

The application of hydrostatic pressure induces FE-to-R crossover, qualitatively changing the dielectric response in figure 24 [55]. Up to ∼3 kbar the main influence of pressure is a shift of T_c to lower temperatures, but above 3 kbar the FE nature of the transition gives way to a relaxor response. The dynamics and energetics of the relaxor state evolve continuously but quickly with increasing pressure [55]. Figure 24 shows that at 15 kbar $\epsilon'(T)$ exhibits the classic relaxor response. Note that there is no thermal hysteresis in T_m, and the low-temperature tetragonal–rhombohedral transition, whose transition temperature increases with pressure at low pressures, has vanished [55].

The 15 kbar results in figure 24 provide a detailed view of the dynamics of the polar domain freezing process; they define relaxation frequencies, f, corresponding to the peak temperature, T_m, and characteristic relaxation times, $\tau = 1/\omega$, where $\omega = 2\pi f$ is the angular frequency. The temperature dependence of τ is found to be non-Arrhenius (figure 25) as is true for most relaxors. It can be fit by the Vogel–Fulcher equation, equation (18) which is applicable to many relaxational phenomena [3]. The fit (solid line) yields values of the parameters in equation (18) that are compatible with those observed for other perovskite relaxors, [3], namely $E = 32$ meV, $T_0 = 353$ K, and $\omega_0 = 4.2 \times 10^{12}$ s^{-1}. E is generally found to decrease with pressure, a manifestation of the decrease in the size of the polar domains with pressure. Simply stated, smaller domains are easier to reorient than larger domains, hence a lower E.

The variety of experimental observations have led to two distinct physical models for PNM and related relaxors in zero field. The first, due to Cross [45], attributes the relaxor

behaviour to a dipolar glass state with randomly interacting polar nanodomains in the presence of random fields. The second, due to Westphal *et al* [56] asserts that PMN is basically a normal FE whose FE macroscopic domains are broken up into nanodomains by the quenched random fields associated with the chemical and charge heterogeneities. It is then the random field interactions that smear the FE transition leading to the *R* state. The literature is full of results and arguments either in favour or against these two models, but the weight of the evidence has recently been in favour of the dipolar glass model, which, in its treatment of the random and frustrated interactions of polar nanodomains, is conceptually easy to accept for relaxors. These two models, as well as a more recent random bond–random field model for relaxors, have been discussed elsewhere [3]. In what follows we restrict our comments on PMN to some very recent neutron scattering results, which have provided some remarkable new insight into the physics of PMN.

Recent inelastic neutron measurements on cubic PMN and its isomorphous analogue, PZN, have revealed a number of remarkable features [57–59]:

(i) anomalous over-damping of the TO phonons, particularly the FE soft mode, below T_d, i.e., when the nanodomains first condense, that only occurs for reduced wavevector q ($\lesssim 0.2\text{Å}^{-1}$). This damping was attributed to the presence of local polar nanoregions (or nanodomains).

(ii) This damping vanishes above T_d where there are no polar nanodomains, and the long wavelength TO modes exhibit normal optic phonon dispersion. This result, thus established a direct connection between the anomalous damping and the nanodomains.

(iii) The soft FE mode recovers, i.e., becomes underdamped, below 220 K, and from there on its energy squared $(\hbar\omega_s)^2$ increases linearly with decreasing T as for normal FEs below T_c (figure 26). Concomitant with this behaviour of the TO soft mode, a strong broadening of the TA phonon starts at T_d and disappears at 220 K, coincident with the recovery of the soft mode. It is noteworthy that 220 K is very close to the temperature $T_c = 213$ K where PMN becomes FE under the threshold biasing field, $E_{th} = 1.8$ kV/cm. The results are summarized in figure 26, where the vertical dashed lines correspond to $T_c = 213$ K and $T_d \cong 625$ K.

These results clearly demonstrate that the lattice dynamics of PMN are intimately connected with the condensation of the polar nanodomains at T_d as well as with a FE transition to presumably a rhombohedral phase below T_c. But how can this be, since it is well established that PMN remains cubic to at least 5 K in the absence of electrical bias? This situation raises the issue of the length scale of the order in this FE state. The authors [58, 59] suggest that PMN undergoes FE ordering that does not achieve long-range order under zero bias, perhaps due to the influence of random fields as well as a phase shift in the atomic displacements in the lattice associated with the presence of the polar domains. In this regard PMN is similar to dilute KTN and Ca-doped $SrTiO_3$ as already discussed in section 3.

4.4. Lead lanthenum zirconate titanate (PLZT) relaxors

Solid solutions of lead zirconate ($PbZrO_3$) and lead titanate ($PbTiO_3$), i.e., $PbZr_{1-y}Ti_yO_3$ or PZT, represent a technologically important family of FEs and antiferroelectrics whose properties and phase transitions have been studied extensively. At high temperatures these materials have the cubic perovskite structure, and on cooling they undergo FE and antiferroelectric (AFE) transitions to lower symmetry phases. Because the isovalent Zr^{4+} and Ti^{4+} are randomly distributed over the B lattice sites, local compositional fluctuations and strain inhomogeneities lead to some broadening of the transitions compared to the pure end members.

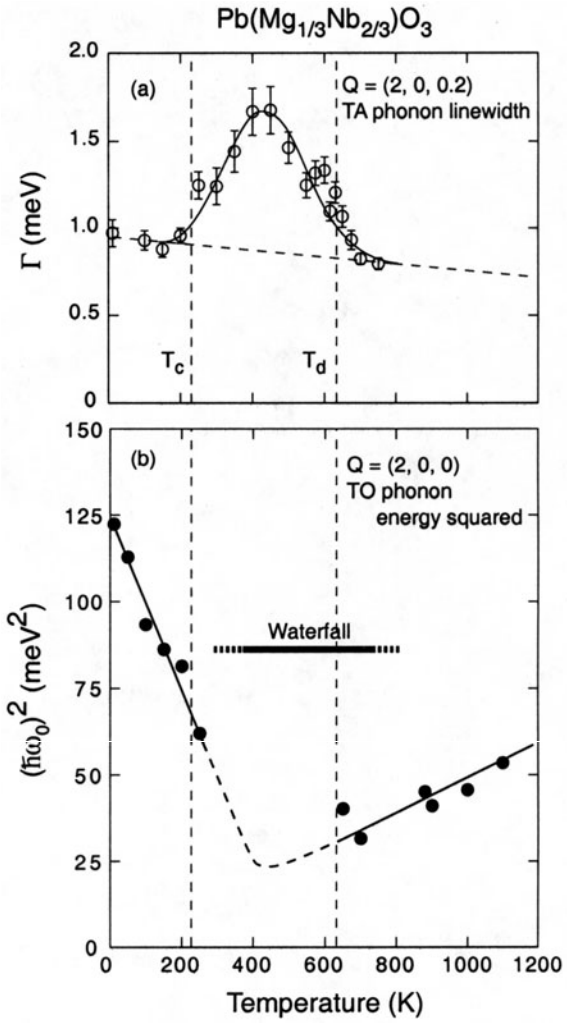

Figure 26. Temperature dependences of (a) the TA phonon linewidth, Γ, and (b) of the square of the TO soft phonon energy, $(\hbar\omega_s)^2$, for PMN. Vertical dashed lines correspond to $T_m = 213$ K and $T_d = 620$ K (after [59]).

However, there are generally no polar relaxational effects (i.e., frequency dispersion) in the audio frequency range, and PZTs exhibit normal, long-range FE and AFE order.

For practical purposes, aliovalent cations are substituted in PZTs at both the A and B cationic sites. For example, La^{3+} is substituted for Pb^{2+} on the A sites to form a well known family of ceramics referred to as PLZT that have unusual dielectric and electro-optic properties [60]. The La^{3+} ions and accompanying vacancies (required to preserve charge neutrality) which are randomly distributed on the A sites break the translational symmetry of the lattice and represent a type of disorder which significantly modifies the properties of these materials. One manifestation of this disorder is the condensation of local, randomly oriented dipolar nanodomains at a temperature (T_d) much higher than the FE transition temperature [3]. These polar nanodomains increase in size as the polarizability of the host lattice increases with decreasing temperature and, for relatively low La^{3+} concentration, ultimately result in the

formation of macroscopic FE domains with long-range polar order. For high concentrations of La^{3+}, on the other hand, the resulting disorder hinders the onset of long-range order, and the polar nanodomains exhibit on cooling slowing down of their polarization fluctuations resulting in a relaxor state at low temperatures.

Relaxor behaviour has been observed in several PLZT compositions [3, 61, 62, 64]. These materials have the chemical formula $(Pb_{1-3x/2}La_x)(Zr_{1-y}Ti_y)O_3$, where the substitution of La^{3+} for Pb^{2+} introduces one A-site vacancy for every two La^{3+} ions. Fairly detailed studies have been made on two La-substituted PZT families:

(i) the $PbZr_{0.65}Ti_{0.35}O_3$ (or PZT 65/35) family denoted by PLZT $x/65/35$, where x is the at.% La. For this material system, relaxor behaviour in the dielectric response becomes experimentally discernible for $x \gtrsim 6\%$, and much of the literature has dealt with compositions $6 \leqslant x \leqslant 9$.
(ii) The $PbZr_{40}Ti_{60}O_3$ (or PZT 40/60) family denoted by PLZT $x/40/60$ for which relaxor response becomes discernible for $x \geqslant 12$ at.% La.

Importantly, these two families represent regions of the PZT phase diagram that exhibit different crystal structures and properties. PZT 65/35 is representative of compositions on the Zr-rich side of the diagram where the cubic PE phase transforms on cooling to a FE rhombohedral phase, the transformation accompanied by relatively little lattice strain. PZT 40/60, on the other hand, is representative of Ti-rich composition where the PE-FE transition is to a tretragonal FE phase, which involves relatively large lattice strain. The relaxor properties of these two PLZT families have been recently reviewed elsewhere [3]. In what follows we restrict our remarks to a few highlights.

First, we note that there is convincing evidence for the existence of polar nanodomains in PLZTs. This is illustrated in figure 27 for PLZT 6/65/35. Shown are the temperature dependences of $1/\epsilon'$ (a), the linear thermal expansion $\Delta\ell/\ell_0$ (b) and the refractive index, $n(c)$. In all cases we see deviations from linear response below ~600 K (the Burns temperature, T_d, where condensation on nanodomains sets in) which is about 170 K above T_m. And while there is a peak in $\epsilon'(T)$ at T_m, there are no anomalies in $\Delta\ell/\ell_0$ and n at this temperature indicating the absence of a bulk phase transition, as is expected for a relaxor.

The usual manner of studying the relaxor properties of PLZTs has been to increase the La^{3+} content and thereby the degree of disorder to induce relaxor behaviour. This is illustrated in figure 28(a) for PLZT $x/40/60$ [62]. Compositions with <12 at.% La exhibit normal FE behaviour as is illustrated by the frequency-independent dielectric response for PLZT 8/40/60. The rounded $\epsilon'(T)$ peak is characteristic of FE ceramics. The FE-to-R crossover occurs at ~12 at.% La, and the 12/40/60 sample was chosen to illustrate the behaviour at this crossover composition at 1 bar. In this case, on cooling the sample enters the relaxor phase, as indicated by the onset of frequency dispersion in $\epsilon'(T)$ as well as in the peak temperature T_m. On further cooling, the sample spontaneously transforms into a FE phase as shown by the arrow. This transformation is thermodynamically first order accompanied by large thermal hysteresis. For compositions above 12 at.% la, the material exhibits classic relaxor behaviour as shown for the 15/40/60 sample.

FE-to-R crossover in fixed PLZT compositions has been induced by the application of hydrostatic pressure. Two specific compositions, PLZT 12/40/60 and PLZT 6/65/35, chosen to be near the FE-to-R crossover for both families have been studied in some detail [3]. The $\epsilon'(T)$ response for PLZT 12/40/60 at different pressures mirrors that at different compositions in figure 28(a). With increasing pressure the relaxor character increases and by 20 kbar the spontaneous R-to-FE transition has vanished and the sample exhibits the classic relaxor response as for the PLZT 15/40/40 at 1 bar in figure 28(a). The pressure-induced FE-to-R

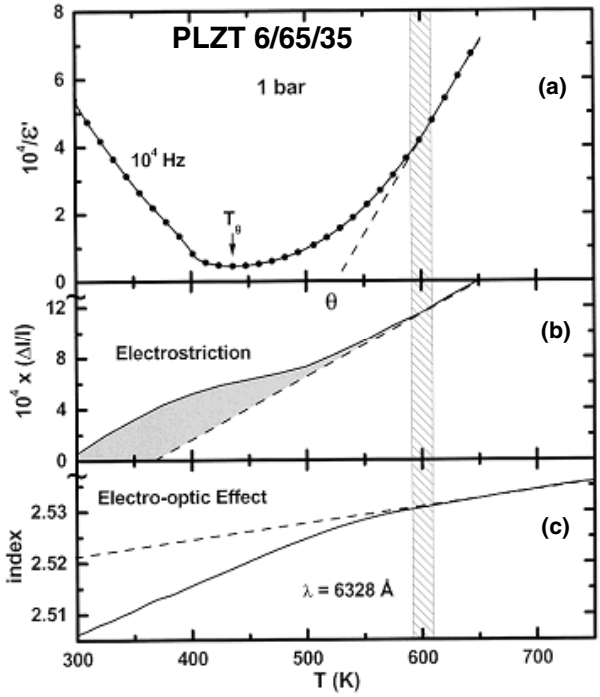

Figure 27. Temperature dependences of $(1/\epsilon')$, the linear thermal expansion $(\Delta\ell/\ell_0)$ and the refractive index (n [46]) for PLZT 6/65/35 showing deviation from linear response at a temperature (T_{Burns}) much higher than T_m (after Samara, unpublished).

crossover has also been observed in PLZT 6/65/35 as shown in figure 28(b). At 1 bar (0 kbar) there is very weak ϵ' dispersion below T_m, and the sample is on the verge of relaxor behaviour. However, on increasing the pressure strong relaxor behaviour sets in by 5 kbar and evolves into a full relaxor response. This is seen in the 10 kbar isobar, which also shows a spontaneous first-order R-to-FE transition at T_c. This transition vanishes at higher pressures, the material exhibiting full relaxor character as seen in the 20 kbar data.

The similarities in the composition-induced and pressure-induced FE-to-R crossover in figure 27 are truly striking. In both cases the crossover results from decreases in the size of and correlations among polar domains. We have already discussed the mechanism by which this happens under pressure. With changing composition, increased substitution increases the degree of host lattice disorder, which disrupts the correlations among polar nanodomains, effectively reducing r_c. Consequently, above a certain concentration of substituents, r_c becomes sufficiently short, the polar clusters never grow to be large enough to percolate most of the sample, and relaxor behaviour sets in at $T \leqslant T_m$. In this concentration regime, the higher the concentration of the substituent, the smaller the effective r_c, and the stronger the frequency dispersion, as observed. Thus, there is an analogy between increasing pressure and increasing substituent content, but it is the pressure results that clarify the physics.

4.5. Field-induced nano-to-macro polar domain transition

As already discussed in section 4.4, the application of a dc biasing electric field can provide much insight into the kinetics and energetics of domain reorientation as well as into the growth

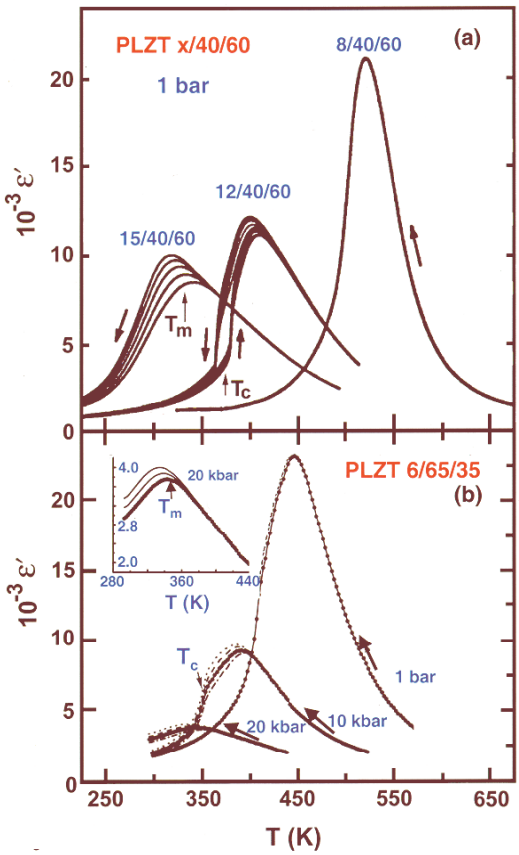

Figure 28. Temperature dependences of ϵ' of (a) PLZT $\chi/40/60$ showing the evolution of the relaxor state with increasing La content x (adapted from [62]) and (b) PLZT 6/65/35 showing the evolution of the relaxor state with pressure (after [3]).

of polar domains. On cooling in the absence of a biasing field, i.e., ZFC, the reorienting polar nanodomains ultimately freeze into an isotropic phase devoid of long-range order, i.e., with random orientations. Here we illustrate some interesting field-induced effects in PLZT 6/65/35 and in PZN–9.5 PT. As noted above, PLZT 6/65/35 is at the FE/R boundary at 1 bar, and the application of even a weak field stabilizes the rhombohedral FE phase. On heating under bias (FH), the sample undergoes a FE-to-PE phase transition. Subsequent cooling from the PE phase under bias (FC) reveals the reverse PE-to-FE transition, but with thermal hysteresis indicating a first-order transition. The dielectric response is essentially frequency independent for both FH and FC cycles as is typical of normal FEs.

Figure 29 shows the influence of 4 kV cm^{-1} bias on the $\epsilon'(T)$ response at 10 kbar [3, 65]. This response is fundamentally different from that at 1 bar. In the absence of bias, this sample exhibits full relaxor character at 10 kbar. On FH at 4 kV cm^{-1} at 10 kbar the sample undergoes a very sharp, dispersionless, first-order phase transition followed by the evolution of a relaxor phase and ultimately a transition to the PE phase. The behaviour is reversed on FC but with a hysteresis of 7 K for the FE transition. Evidently the field increases r_c just enough at 10 kbar to strengthen the collective behaviour of the polar domains and stabilize the FE phase. On heating r_c decreases just enough to result in a spontaneous phase transition at T_c following

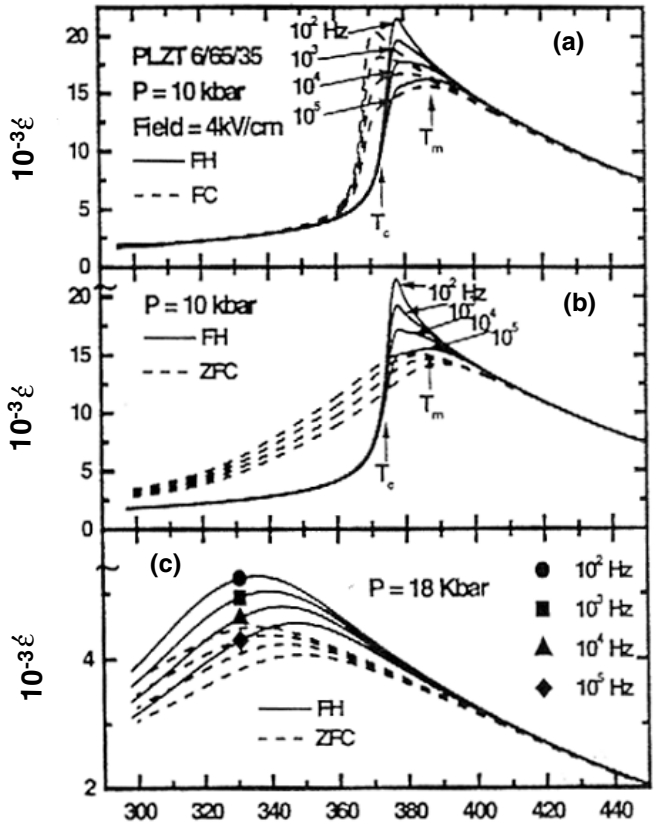

Figure 29. Temperature dependence of ϵ' of PLZT 6/65/35 at 10 and 18 kbar showing the influence of a 4 kV cm^{-1} dc biasing electric field under various field (F) and ZF heating (H) and (C) conditions (after [3, 65]).

which r_c becomes too short to sustain long-range order and results in an R phase, which on continued heating transforms to the PE phase. The sequence is reversed on FC. Figure 29(b) shows the 10 kbar response at 4 kV cm^{-1} for both FH (which is identical to that in figure 29(a)) and ZFC. The results show that in the absence of bias (ZFC) the sample reveals its true ground state, which is a relaxor.

At a still higher pressure (18 kbar, figure 29(c)) the response changes qualitatively. At this pressure r_c and the polar domains are too small for a 4 kV cm^{-1} field to overcome the random freezing of the domains. Consequently, only the R phase is observed under FC and FH conditions as well as in the absence of a bias.

As discussed in section 4.3, pressure induces a FE-to-R crossover in PZN–9.5 PT. The crossover evolves with pressure and is well established by 5 kbar in the absence of a biasing field. Modest fields can, however, restabilize the FE phase, a nano-to-macrodomain transition [55]. Figure 30 shows some results at 5 kbar. Prior to this experiment, the sample was cooled at 4 kV cm^{-1} from 420 to 77 K and then field heated at the same field to 300 K after which the field was removed. This combination of FC/FH stabilized the FE phase as is clearly shown by the subsequent 300–550 K ZFH scan in figure 30, which is a characteristic FE response. Subsequent ZFC from 550 K reveals the full relaxor (nanodomain) character of the

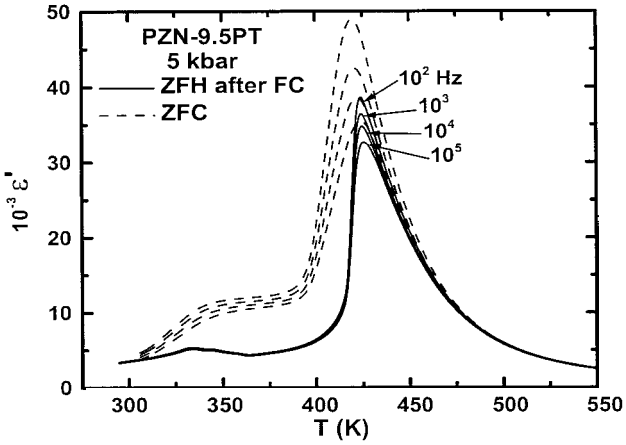

Figure 30. Temperature dependence of ϵ' of PZN–9.5 PT at 5 kbar on ZFH after FC at 4 kV cm^{-1} followed by ZFC (after [55]).

sample, which is the ground state in the absence of bias. The ZFC scan in the figure also shows the $\epsilon'(T)$ shoulder associated with the low-T tetragonal-to-rhombohedral transition [55].

5. Concluding remarks

This review has focused on the relaxational properties of compositionally disordered ABO_3 perovskite oxides. These oxides are the prototypical soft FE mode systems, and their interesting dipolar relaxational properties are determined by their long, strongly temperature-dependent correlation lengths for dipolar interactions. The simplest cases involve dilute (<0.1 at.%) chemical substitutions in the incipient FEs $KTaO_3$ and $SrTiO_3$, which exhibit relatively weak, low-temperature Debye-type relaxations. More complicated dipolar interactions are seen in Li- and Nb-doped $KTaO_3$ with dopant concentrations up to a few at.%, which exhibit glass-like relaxor (R) and relaxor-to-ferroelectric (FE) crossover behaviours at low temperature. Finally, there is a class of more complex perovskites represented by PMN, PZN-PT and the PLZTs that exhibit strong, high-temperature relaxor and/or FE properties. The relaxational properties of these different classes were reviewed briefly, and it was shown that these properties are determined and can be understood in terms of soft mode response. It was also shown that hydrostatic pressure, biasing dc electric fields as well as the interplay between them have provided much insight into the physics.

Relaxors have been one of the 'hot' topics in ferroelectricity during the recent past. The exceptionally large dielectric susceptibilities, electromechanical coupling coefficients and electro-optic constants of perovskite relaxors have been subjects of intense scientific and technological interest. The scientific challenges and technological potential of these materials will ensure that this field will continue to be quite active for the foreseeable future.

Acknowledgments

I express my deep appreciation to Mrs Angel Jimenez for her support in preparing the manuscript (her cheerful attitude made the task enjoyable) and to my colleague Eugene Venturini for a careful reading of the manuscript.

This work was supported by the Division of Materials Sciences and Engineering, Office of Basic Energy Sciences, US Department of Energy. Sandia is a multiprogram laboratory operated by Sandia Corporation, a Lockheed Martin Company, for the DOE under contract DE-AC04-94AL85000.

References

[1] Lines M E and Glass A M 1977 *Principles and Applications of Ferroelectrics and Related Materials* (Oxford: Clarendon)
[2] Samara G A and Peercy P S 1981 *Solid State Physics* vol 36, ed H Ehrenreich, R Spaepen and D Turnbull (New York: Academic) p 1 and reference therein
[3] Samara G A 2001 *Solid State Physics* vol 56, ed H Ehrenreich and F Spaepen (New York: Academic) p 240 and references therein
[4] Frohlich H 1958 *Theory of Dielectrics* (Oxford: Oxford University Press) p 70
[5] Fischer B and Klein M W 1976 *Phys. Rev. Lett.* **37** 756
[6] Aharony A 1978 *Solid State Commun.* **28** 667
[7] Vugmeister B E and Glinchuk M D 1990 *Rev. Mod. Phys.* **62** 993 and references therein
[8] Fiory A T 1971 *Phys. Rev.* B **4** 614
[9] Medina R, Nava R and Saint-Paul M 1984 *Solid State Commun.* **50** 51
[10] Salce B, Gravil J L and Boatner L A 1994 *J. Phys.: Condens. Matter* **6** 4077 and references therein
[11] Müeller K A and Burkard H 1979 *Phys. Rev.* B **19** 3593
[12] Uwe H, Lyons K B, Carter H L and Fleury P A 1986 *Phys. Rev.* **33** 6436
[13] Prater R L, Chase L L and Boatner L A 1981 *Phys. Rev.* B **22** 221
[14] Vogt H 1991 *J. Phys.: Condens. Matter* **3** 3697
[15] Nowick A S, Fu S Q, Lee W K, Lin B S and Scherban T 1994 *Mater. Sci. Eng.* B **23** 19
[16] Laguta V V, Glinchuk M D, Bykovi P, Rosa U, Jsastrabik L, Savinov M and Trybula Z 2000 *Phys. Rev.* B **61** 3897–904
[17] Bidault O, Maglione M, Actis M, Kchikech M and Salce B 1995 *Phys. Rev.* B **22** 4191
[18] Trepakov V, Smutng F, Vikhnin V, Bursian V, Sochava, Jastrabik L and Syrnikow R 1995 *J. Phys.: Condens. Matter* **7** 3765
[19] van der Klink J J and Borsa R 1984 *Phys. Rev.* B **30** 52
[20] Bykov I P, Geifman I N, Glinchuk M D and Krulikovskii B K 1980 *Fiz. Tverd. Tela (Leningrad)* **22** 2144 (Engl. transl. 1980 *Sov. Phys.–Solid State* **22** 1248)
Bykov I P, Geifman I N, Glinchuk M D and Krulikovskii B K 1985 *Fiz. Tverd Tela (Leningrad)* **27** 1908 (Engl. transl. 1985 *Sov. Phys.–Solid State* **27** 1149)
[21] Abraham M M, Boatner L A, Olson D N and Höchli U T 1984 *J. Chem. Phys.* **81** 2528
[22] Siegal E and Müller K 1979 *Phys. Rev.* B **19** 109
[23] Samara G A and Boatner L A 2000 *Phys. Rev.* B **61** 3889–96
[24] Leung K 2001 *Phys. Rev.* B **63** 134415-1–11
[25] Höchli U T, Knorr K and Loidl A 1990 *Adv. Phys.* **39** 405
[26] Chow H, Shapiro S M, Lyons K B, Kjems J and Rytz D 1990 *Phys. Rev.* B **41** 7231
[27] Foussadier L and Fontana M D 1996 *Ferroelectrics* **184** 277
[28] Vogt H 1996 *Ferroelectrics* **184** 31
Vogt H 1997 *Ferroelectrics* **202** 157
[29] Kleemann W, Kutz S and Rytz D 1987 *Europhys. Lett.* **4** 239
[30] Toulouse J and Pattnaik R 1998 *J. Korean Phys. Soc.* **32** S942
[31] Yacoby Y and Just S 1974 *Solid State Commun.* **12** 715
[32] Doussineau P, Farssi Y, Frenois C, Levelut A, McEnaney K, Toulouse J and Ziolkiewicz 1993 *Europhys. Lett.* **24** 415
[33] Samara G A 2002 *Mater. Res. Soc. Symp. Proc.* **718** 281 and references therein
[34] Kleemann W, Schäfer F J and Rytz D 1985 *Phys. Rev. Lett.* **54** 2038
[35] Lyons K B, Fleury P A and Rytz D 1986 *Phys. Rev. Lett.* **57** 2207
[36] Toulouse J, DiAntonio P, Vugmeister B E, Wang X M and Knauss L A 1993 *Phys. Rev. Lett.* **68** 232
[37] Andrews S R 1985 *J. Phys. C: Solid State Phys.* **18** 1357
[38] Hanske-Petipierre O, Yacoby Y, Mustre-de Leon J, Stern E A and Rehr J J 1991 *Phys. Rev.* B **44** 6700
[39] Samara G A 1985 *Japan. J. Appl. Phys. (Suppl.)* **24** 80
[40] Bianchi U, Dec J, Kleemann W and Bednorz J G 1995 *Phys. Rev.* B **51** 8737

[41] Kleemann W, Albertini A, Kuss M and Lindner R 1997 *Ferroelectrics* **203** 57
[42] Bednorz J G and Müller K A 1984 *Phys. Rev. Lett.* **52** 2289
[43] Venturini E L, Samara G A and Kleemann W 2003 *Phys. Rev.* B submitted
[44] Vakhrushev S B *et al* 1989 *Ferroelectrics* **90** 173
Schmidt G *et al* 1981 *Phys. Status Solidi* a **63** 501
[45] Cross E 1987 *Ferroelectrics* **76** 241
[46] Burns G and Dacol F H 1983 *Solid State Commun.* **48** 853
Burns G and Dacol F H 1985 *Phase Transit.* **5** 261
[47] Binder K and Young A P 1986 *Rev. Mod. Phys.* **58** 801
[48] Sherrington D and Kirkpatrick S 1975 *Phys. Rev. Lett.* **35** 1972
[49] Viehland D, Wuttig M and Cross L E 1991 *Ferroelectrics* **120** 71
Viehland D, Wuttig M and Cross L E 1993 *Ferroelectrics* B **46** 8003 and references therein
[50] Ye Z G and Schmid H 1993 *Ferroelectrics* **145** 83
[51] Ye Z G 1996 *Ferroelectrics* **184** 193
[52] Mulvihill M L, Park S E, Risch G, Li Z, Uchino K and Shront T R 1996 *J. Appl. Phys.* **35** 3984
[53] Park S E and Shrout T R 1997 *J. Appl. Phys.* **82** 1804 and references therein
[54] Colla E V, Yushin N K and Viehland D 1998 *J. Appl. Phys.* **83** 3298 and references therein
[55] Samara G A, Venturini E L and Schmidt V H 2001 *Phys. Rev.* B **63** 184104
[56] Westphal V, Kleemann W and Glinchuk M D 1992 *Phys. Rev. Lett.* **68** 847
[57] Gehring P M, Park S E and Shirane G 2000 *Phys. Rev. Lett.* **84** 5216
Gehring P M, Park S E and Shirane G 2000 *Phys. Rev.* B **63** 224109
[58] Gehring P M, Wakimoto S, Ye Z G and Shirane G 2002 *Phys. Rev. Lett.* (*Preprint*)
[59] Wakimoto S, Stock C, Ye Z G, Chen W, Gehring P M and Shirane G 2002 *Phys. Rev. Lett.* (*Preprint*)
[60] Haertling G H and Land C E 1971 *J. Am. Ceram. Soc.* **54** 1
See also
Haertling G H 1978 *Ferroelectrics* **75** 25
[61] Viehland D, Li J F, Jang S J, Cross L E and Wuttig M 1992 *Phys. Rev.* B **46** 8013
Viehland D, Li J F, Jang S J, Cross L E and Wuttig M 1992 *Phys. Rev.* B **46** 8003
[62] Dai X, DiGiovanni A and Viehland D 1993 *J. Appl. Phys.* **74** 3399
See also
Dai X *et al* 1994 *Phil. Mag.* B **70** 33
[63] Krumins A, Shiosaki T and Koizumi S 1994 *Japan. J. Appl. Phys.* **33** 4940
[64] Bobnar V, Kutnjak Z, Pirc R and Levstik A 1999 *Phys. Rev.* B **60** 6420
[65] Samara G A 2000 Fundamental physics of ferroelectrics *Aspen Center for Physics Winter Workshop* ed R E Cohen (New York: American Institute of Physics) p 344